國 立 交 通 大 學

光 電 工 程 研 究 所

碩 士 論 文

氮化銦薄膜與金奈米顆粒之非線性光學特性

Optical Nonlinearity of InN film and Gold nanoparticles

研 究 生：張晏銘

指導教授：安惠榮 教授

中 華 民 國 一 零 零 年 九 月

氮化銦薄膜與金奈米顆粒之非線性光學特性

Optical Nonlinearity of InN film and Gold nanoparticles

研 究 生：張晏銘　　Student：Yen-Ming Chang 指導教授：安惠榮 教授　　Advisor：Prof. Hyeyoung Ahn

國 立 交 通 大 學

光電工程研究所

碩 士 論 文

A Thesis

Submitted to Department of Photonics and

Institute of Electro-Optical Engineering

College of Electrical Engineering

National Chiao Tung University

In partial Fulfillment of the Requirements

for the Degree of

Master of Science

in

Electro-Optical Engineering

September 2011

Hsinchu, Taiwan, Republic of China

中華民國一 零 零 年 九 月

Optical Nonlinearity of InN film and Gold nanoparticles

Student :Yen-Ming Chang Advisors : Prof. Hyeyoung Ahn

Department of Photonics and Institute of Electro-Optical Engineering
National Chiao Tung University

Abstract

While the fundamental physical properties of indium nitride (InN) has been intensely studied since the first demonstration of its narrow bandgap (~0.6 eV), its nonlinear properties are relatively not well known. Metal nanomaterials have attracted great attention in the fields of plasmonics and metamaterials due to the excellent characteristics of large nonlinearity and tunability of size-dependent resonant wavelength. In particular, metal nanomaterials have the high third-order nonlinear susceptibility and the interaction with light induces large change in their refractive index and absorption. We applied the Z-scan technique to investigate the nonlinear optical properties of InN and 3-dimensional Au nanoparticle supercrystals.

In the experiment of the InN film, we successfully measured the nonlinear optical parameters at two wavelengths; the nonlinear refractive index $n_2=(5.84 \pm 0.2) \times 10^{-11}$ and nonlinear absorption coefficient $\beta=-(2.12 \pm 0.06) \times 10^{-6}$ at 800 nm and $n_2=(1.86 \pm 0.1) \times 10^{-10}$, $\beta=(1.65 \pm 0.01) \times 10^{-5}$ at 1550 nm, near the bandgap of InN. The opposite sign of nonlinear absorption coefficients is explained by the competition of different absorption processes such as the band filling effect at 800 nm and the band-gap renormalization effect at 1550 nm. In the measurement of 3D Au nanoparticle structures with a high repetition rate (80 MHz) laser, accumulated

thermal effect elevated the sample temperature above the melting temperature, which is lower than that of Au film, and prevents the determination of the nonlinear coefficients. With a low repetition rate laser (1 kHz), however, the Z-scan signal-like responses were obtained only when the laser power is over a threshold value. Large peak intensity permanently damaged the samples and the morphology changes depend on the conditions of lasers such as pulsewidth and repetition rate.

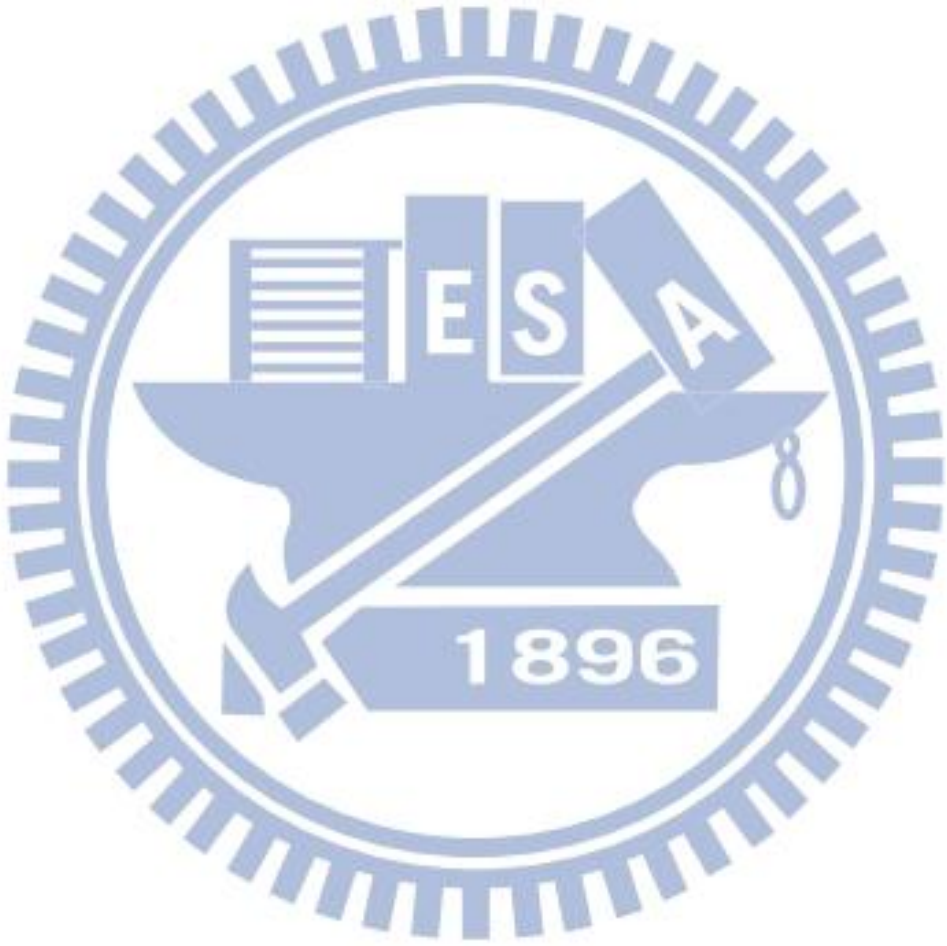

誌謝

在這兩年多的碩士班研究生活中,第一個要感謝的是我的指導教授安惠榮老師的指導,讓我能順利完成論文,老師總是在我們遇到瓶頸時提供適當的意見與耐心地討論讓我能順利完成實驗,此外,老師不斷強調我們的學習態度,使我學習到對事情積極和負責的態度。其次,我要感謝我們實驗室的李弘貿博士,李博士總是很樂意和我討論問題(不論是課內或課外),也特別感謝他常常在假日的時候抽空,帶我到清大做實驗。再來,我要感謝已經畢業的靖中、大支學長和苡柔學姊,讓我們的碩一生活如此有趣,然後也跟你們學到不少實驗技巧和經驗,也謝謝我的同學,至正和賈哥,在安排實驗的時間上我們會彼此體諒,並且常在實驗有困難時互相討論和幫助,另外還有我的學弟妹們,李澤、紀瑩、安佳、育昇和東閔,謝謝他們對實驗室的貢獻,也很感謝李澤學弟在我生活上的幫助,還有謝謝隔壁實驗室的同學,在假日或晚上做實驗時,我們互相加油打氣。最後我要感謝我的家人,讓我能無後顧之憂地完成碩士學位,謝謝他們的栽培和支持,接下來就是我孝順你們的時候。

Content

List of Figures

List of Table

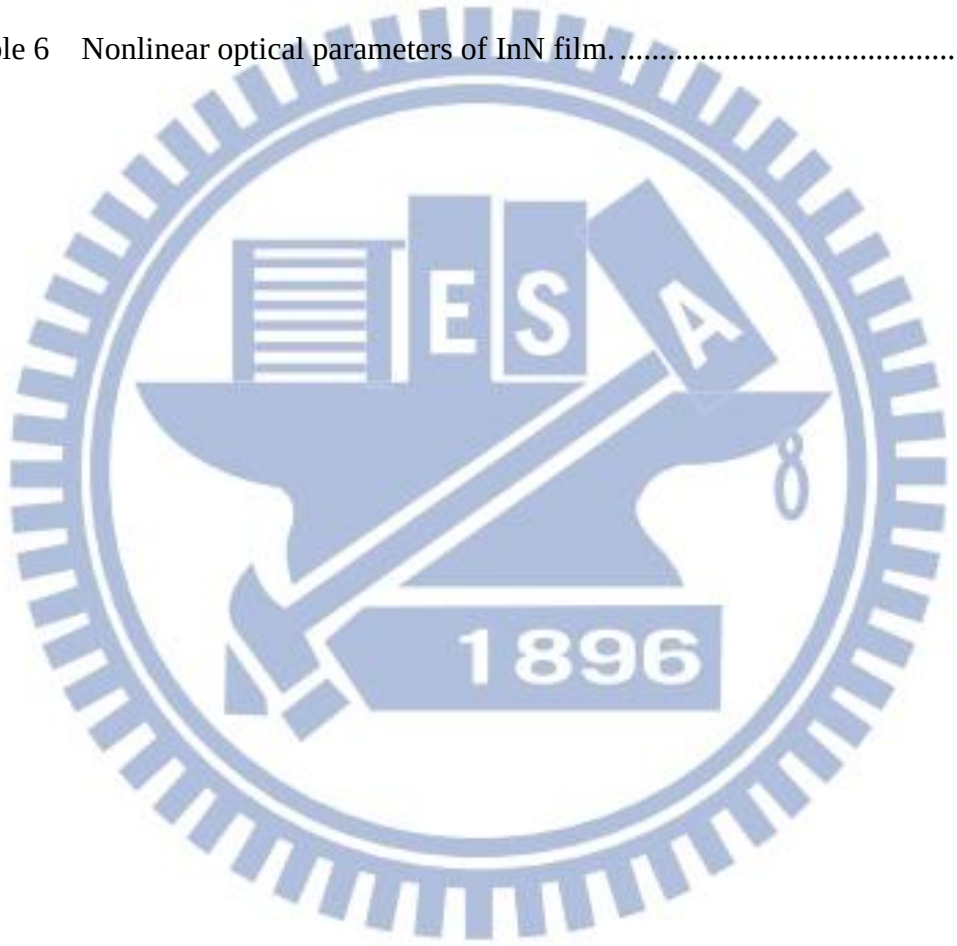

Chapter 1 Introduction

In the past decade, optical nonlinear materials have attracted great attention and nonlinear optical effects based on different absorption processes have been useful for many different applications, such as optical switch[1-1], ultrafast laser systems, optical limiting devices[1-2]. The characterization of the nonlinear optical properties is of great interest in these applications. Since it was developed by Sheik-Bahae et al. in 1990 Z-scan technique[1-3] has been the most popularly used experimental method for measuring material nonlinearities due to its high sensitivity, simplicity of experimental setup and numerical analysis. The Z-scan method can be used for the determination of the sign and the magnitudes of the complex third-order nonlinear susceptibility, $\chi^{(3)}$. The real and imaginary parts of $\chi^{(3)}$ correspond to the nonlinear refractive index and the nonlinear absorption coefficient, respectively, which are critically important to evaluate the merits of the optical nonlinear materials.

Indium nitride (InN) combined with other III-V nitrides has great potential applications in high-frequency electronic devices, near-infrared optoelectronics, and high-efficiency solar cells. Recently, there has been growing interest on the nonlinear properties of InN which may induce optical limiting or optical damage. We used the Z-scan technique to obtain third-order nonlinear refractive index n_2 and nonlinear absorption coefficient β of InN at two different wavelengths 800 nm and 1550nm. Since 800 nm (E~1.5 eV) and 1550 (E~0.8 eV) are far above and close to the bandgap energy of InN (E_g~0.6), respectively, excess energy-dependent nonlinear absorption process can be identified.

Recently, metal nanomaterials have attracted great attention in the fields of plasmonics and metamaterials due to the excellent characteristics of large nonlinearity and tunability of size-dependent resonant wavelength. In particular, metal

nanomaterials have the high third-order nonlinear susceptibility and the interaction with light induces large change in their refractive index and absorption. Up to now, optical properties of metamaterials based on metal nanomaterials have been intensely investigated, but most of measurements were performed on two-dimensional (2D) arrays or waveguides. However, for the development of practical devices, it is required to have three-dimensional (3D) structures that are thick enough to hold the bulk or bulk-like properties. Several 3D optical metamaterials have been demonstrated by using layer-by-layer stacking technique, however, large-scale 3D metamaterials can be realized only by self-assembly method. Recently, large-area (>1 cm^2), 3D gold and silver nanoparticle supercrystal films were successfully synthesized from suspensions of thiolate-passivated gold or silver colloids by using layer-by-layer self-assembly method. Reflectance spectra from these films show that plasmonic longitudinal and transverse modes can be observed for the supercrystal films with larger than 10 monolayers, indicating that films with this thickness regime have the bulk-like properties. Increase of thickness can enhance the optical nonlinearity and the transmission and reflection of the 3D Au nanoparticle films can be accordingly changed. Previous works have already demonstrated the optical nonlinear properties of Au nanoparticles in 2D structures, however, those of 3D structures are still unknown.

We tried to elucidate the morphology changes of Au nanoparticle supercrystals by using the SEM imaging and the Z-scan method based on Ti:sapphire laser with MHz an kHz repetition rates. However, accumulated thermal effect preventes the measurement of nonlinear coefficient from Au nanoparticles. Instead, we studied the influence of laser parameters to the morphology change of nanoparticle multilayers.

1-1 Basics of optical device

The nonlinearity in material is important to the practical applications. In this section, we will introduce the operation of all-optical switch and optical limiting.

1-1-1 All-optical switching

Photonic integrated circuits have recently been demonstrated in silicon. However, these structures are usually passive. All-optical switches and modulators have been demonstrated by employing III-V compound materials based on photoexcited free carrier concentrations resulting from linear or two-photon absorption. Therefore, in an all-optical switch, the delicate modulation of light to control the nonlinearity of optical devices is crucial. For example, a Mach-Zehnder interferometer[1-5] with nonlinear optical element in one of its branches may be used as an all-optical 1×2 switch directing an optical beam at one of its two input ports to either of its output ports as shown in [figure 1-1]. In the absence of the control beam, the interferometer is balanced such that the input light is directed to one of output ports. When the control beam is applied, it induces a change in refractive index, which in turns creates an incremental phase shift of π so that the input beam is directed to the other output port. The switching time is another important controlling factor. The shorter switching time, the faster signal processing we get. The switching time of all-optical switches is typically in the order of ps.

An effective all-optical switch requires the nonlinear optical materials with large nonlinear refractive index and absorption coefficient. InN, a III-V material with a narrow bandgap energy, can be a good candidate for all-optical switches and we used the Z-scan method to measure the nonlinear optical parameters.

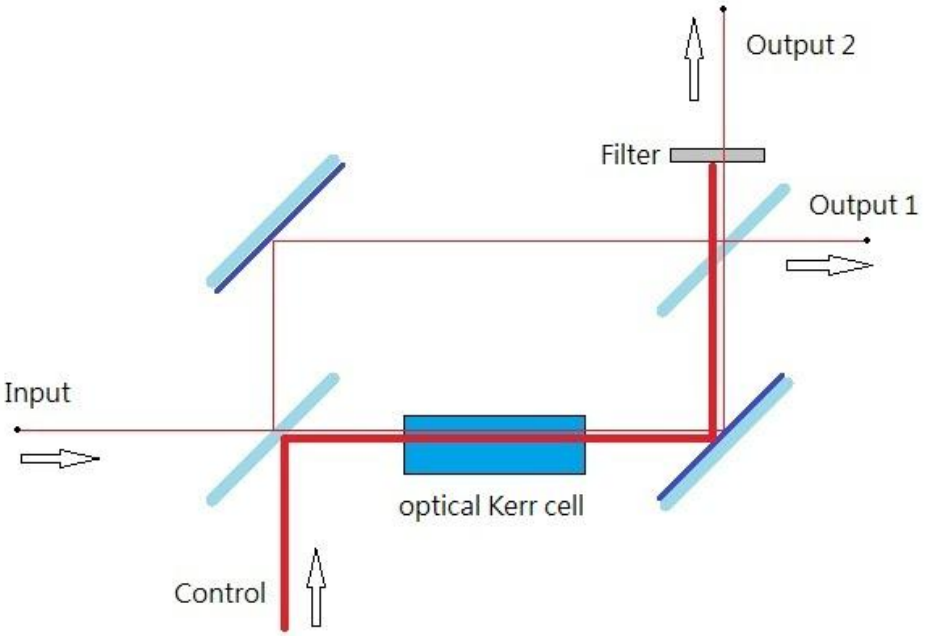

Fig. 1-1 An all-optical 1×2 switch using a Mach-Zehnder interferometer with an optical Kerr cell.[1-5]

1-1-2 Optical limiting

Optical limiters are devices designed to have high transmittance for low level inputs while blocking the transmittance for high intensity laser beams. Optical limiting device can be used for protection of human eyes or optical sensors against high-intensity laser radiation-induced damage. This kind device generally can be classified into two broad categories: one is the energy-spreading type of device, and the other is the energy-absorbing type of device. The principle of the first type of device is based on nonlinear refractive index which causes self-focus effect as laser beam passing through the nonlinear sample. At low intensity, the nonlinear effect is negligible and all laser beam can be detected through a properly placed aperture in front of a detector. At high intensity, self-focus effect causes the laser beam diverse and only a small fraction of beam can pass through the aperture. Finally, the detector can be protected from the damage. The principle of second type of device is based on nonlinear absorption that absorption of material increases along with the increase of

exciting intensity and limits the amount of energy through the material. These nonlinear absorption materials can be used not only for optical limiting but also for optical stabilization purposes. A random intensity fluctuation of the laser signals will be reduced and make signal smooth after passing through material. This characteristic can be applied in optical telecommunications and optical data processing.

1-2 Z-scan Technique

In this section, we will derive optical Kerr effect and then introduce the operation of Z-scan technique.

1-2-1 Optical Kerr effect

In the case of linear optics, the induced polarization depends linearly on the electric field strength in a manner that can be described [1-6]

$$P = \varepsilon_0 \chi^{(1)} E$$

where the constant of proportionality $\chi^{(1)}$ is known as the linear susceptibility. In nonlinear optics, the nonlinear optical response can often be written in the form

$$P = \varepsilon_0 \chi^{(1)} E + 2dE^2 + 4\chi^{(3)} E^3 + \cdots$$

where d and $\chi^{(3)}$ are coefficients describing the strength of the second and third-order nonlinear effect. We can write the polarization density as a sum of linear and nonlinear parts,

$$P = \varepsilon_0 \chi^{(1)} E + P_{NL}$$

$$P_{NL} = 2dE^2 + 4\chi^{(3)} E^3 + \cdots$$

In centrosymmetry medium, the second-order nonlinear term is absent. The dominant nonlinearity is third order,

$$P_{NL} = 4\chi^{(3)} E^3$$

In considering the simple case, the applied field is monochromatic, the nonlinear polarization P_{NL} contains a component at frequency ω and at frequency 3ω,

$$P_{NL}(3\omega) = \chi^{(3)}E^3$$

$$P_{NL}(\omega) = 3\chi^{(3)}|E|^2E$$

The first term describes a response at frequency 3ω and it leads to the process of third-harmonic generation. The polarization component at frequency ω corresponds to a change of susceptibility $\Delta\chi$ given by

$$\epsilon_0\Delta\chi = 3\chi^{(3)}|E|^2 = 6\chi^{(3)}\eta I$$

where $I=\frac{|E|^2}{2\eta}$ is optical intensity. Since $n^2 = 1+\chi$, we have $2n\Delta n=\Delta\chi$ so Δn can be expressed as

$$\Delta n = \frac{3\eta}{\epsilon_0 n}\chi^{(3)} I \equiv n_2 I$$

where

$$n_2 = \frac{3\eta_0}{\epsilon_0 n^2}\chi^{(3)}$$

.

The overall refractive index can be written as

$$n(I) = n_0 + n_2 I \qquad (1\text{-}1)$$

This effect is called **optical Kerr effect**. The change in refractive index is proportional to optical intensity. An optical wave traveling in a third-order nonlinear medium will cause Self-Phase Modulation, Self-Focusing, and Spatial Solitons. The Z-scan technique is primarily used Self-focusing of material to measure the change of refractive index.

1-2-2 Z-scan method

When a Gaussian laser beam pass through a Kerr medium, the overall refractive index can be written as

$$n(I) = n_0 + n_2 \frac{cn_0}{2\pi} |E|^2 \frac{\omega_0^2}{\omega^2(z)} e^{-\frac{2r^2}{\omega^2(z)}}$$

and then, the nonlinear refractive index n is proportional to e^{-r^2}. Assuming n_2 is positive, the refractive index at the center of sample would be larger than that at the side and gradually decrease approaching the side of the sample. So the sample can act like a focus lens as laser beam going through. This effect is known as self-focusing. On the contrary, the sample can act like a divergence lens and defocus the beam when n_2 is negative. The Z-scan technique is primarily based on the spatial beam distortion, which is caused by sample's self-focusing characteristics. Figure 1-2 shows a typical Z-scan experimental setup; focused Gaussian laser beam passes through a sample that is mounted on a step-motor and we measure the transmittance through an aperture in the far field.

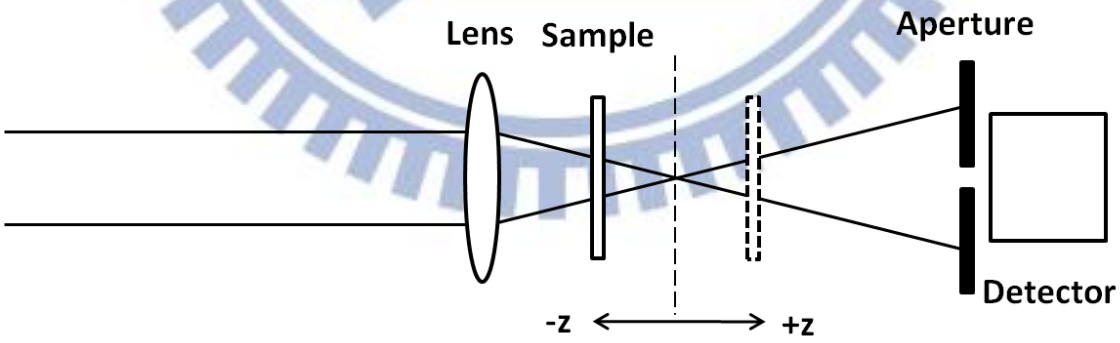

Fig. 1-2 Basic experimental setup of Z-scan

For a material with purely positive nonlinear refraction (no nonlinear absorption and $\Delta n > 0$), when the material is far from the focus, optical transmittance remains constant because the beam irradiance is too low to induce nonlinear refraction. As the

material is brought close to focus, the beam irradiance beomes high enough to cause self-focusing in the material. Before reaching the focal point, the high-irradiance light induces the self-focusing which moves the focal position closer to lens and results in a greater divergence in the far field. And the transmittance through the aperture is reduced. When the material is placed after focus, the self-focusing tend to collimate the beam, causing the increase of the transmittance through the aperture. As the material is moved away from focus, transmittance become constant since the irradiance is low again. So the Z-scan traces will have a valley-peak configuration. In the same analysis, the Z-scan trace of the negative nonlinear refraction ($\Delta n < 0$) shows a peak-valley configuration, as depicted in Figure 1-4. We call this process as "close-aperture (CA) Z-scan".

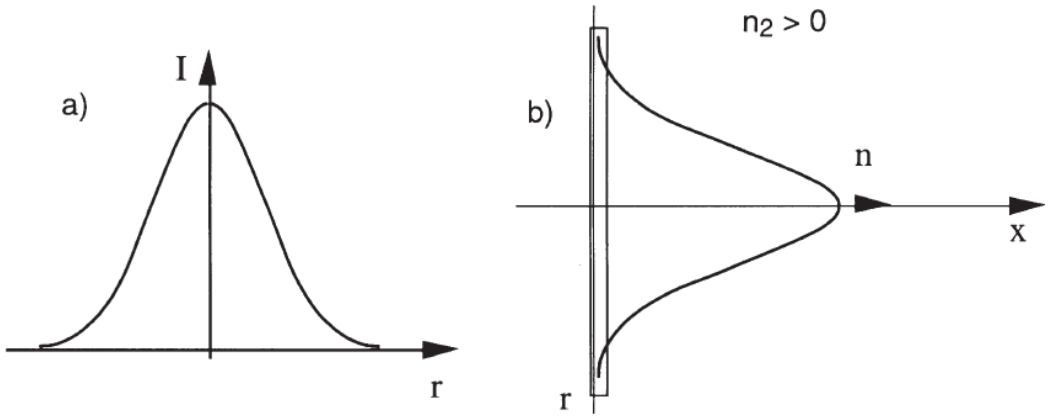

(c)

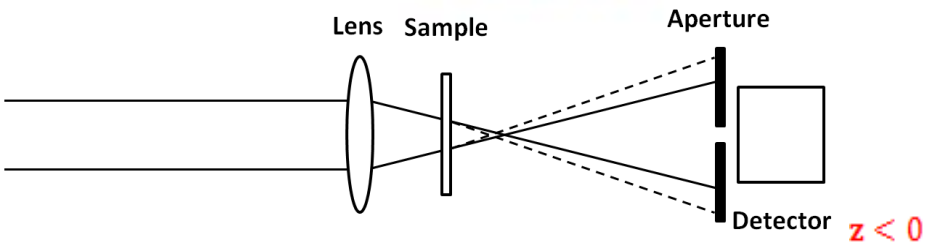

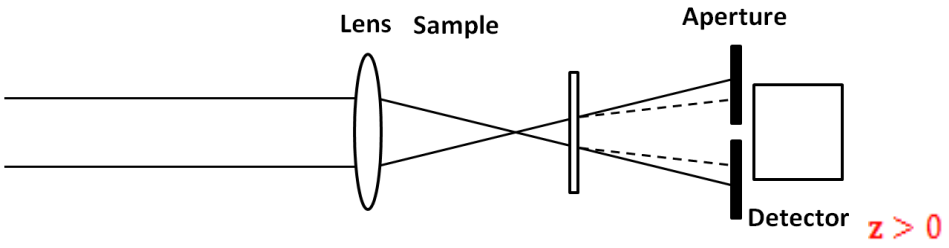

Fig. 1-3 Description of Z-scan technique:

(a) Gaussian beam intensity distribution as a function of radial distance.[1-7]

(b) Assuming the propagation of this intensity distribution along the *x* direction in a thin slab of $\chi^{(3)}$ material, the variation of the index of refraction follows the intensity distribution along the diameter. Depending on the sign of the nonlinear index of refraction, the index of refraction increases ($n_2 > 0$) or decreases ($n_2 < 0$) when going toward the center of the laser beam,

(c) illustrates the Z-scan configuration described above. (Assume $n_2 > 0$)

The sensitivity of the Z-scan to nonlinear refraction is due to the aperture before the detector. If we remove the aperture, the detector will collect all the transmittance and therefore is insensitive to the beam distortion which is caused by nonlinear refraction. Instead, the Z-scan signal would be sensitive to the nonlinear absorption. In considering the nonlinear absorption, absorption coefficient can be written as $\alpha = \alpha_0 + \beta I$ and we can expect that the Z-scan traces would be symmetric to the focus, as shown in Figure 1-5. We called this process as "open-aperture (OA) Z-scan". For OA Z-scan, the nonlinear refraction and nonlinear absorption are present simultaneously. For example, multiphoton absorption will enhances the valley and suppresses the peak and the configuration would not be symmetric. To extract nonlinear refraction signal from this data, a further OA Z-scan is necessary and let CA Z-scan be divided by it. We can easily get pure nonlinear refraction component from

the result of this procedure without complex computer fitting. Figure 1-6 is an example to show how to extract nonlinear refraction signal when nonlinear refraction and nonlinear absorption present simultaneously.

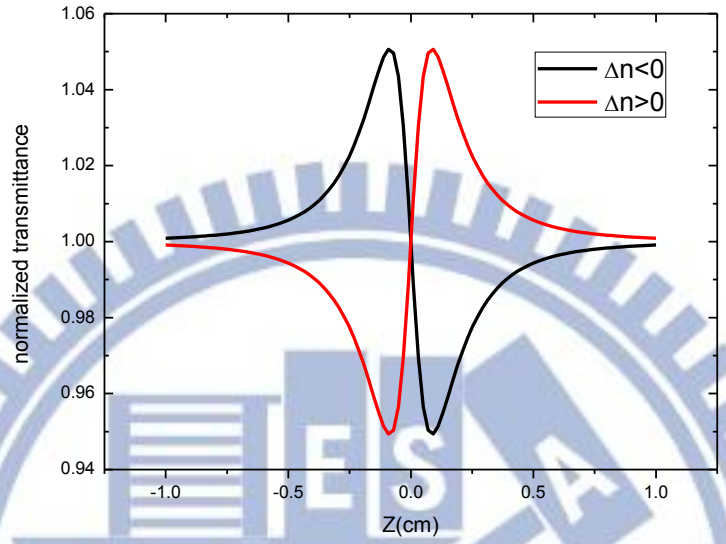

Fig. 1-4 shows close-aperture Z-scan traces with different nonlinear refraction. $n_2 > 0(red\ line)$ $n_2 < 0(black\ line)$

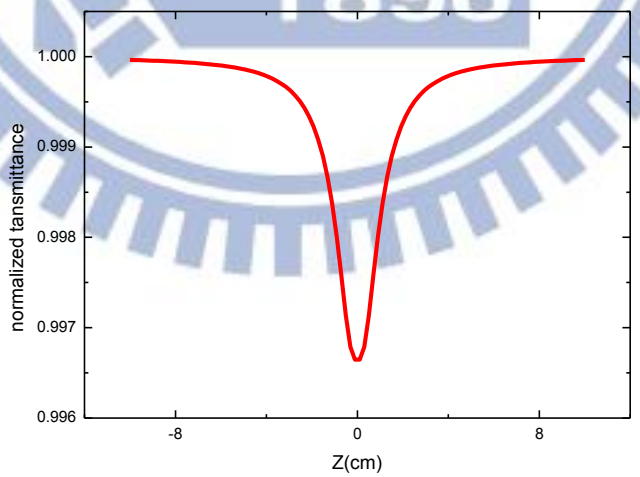

Fig. 1-5 is a typical open-aperture Z-scan traces and shows a increase of absorbance as material approaching focus. (β>0)

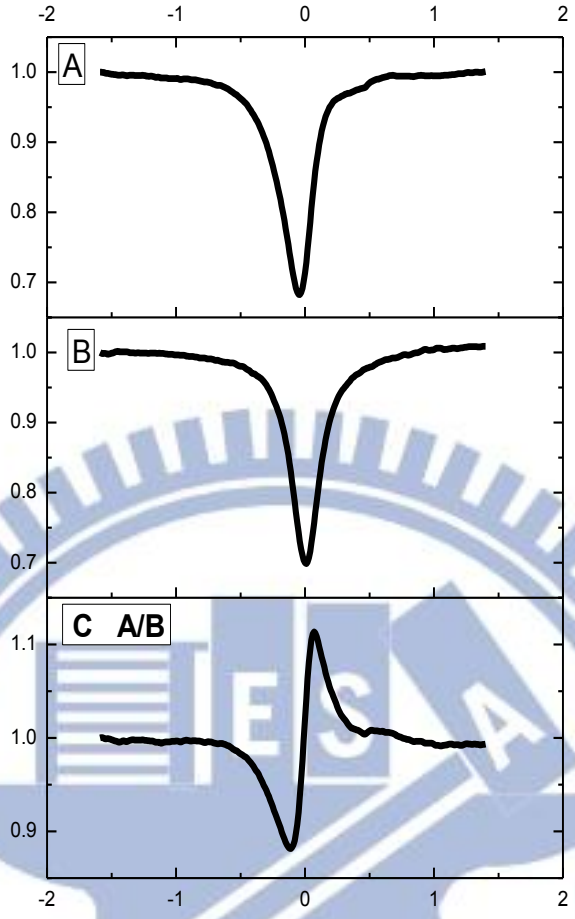

Fig. 1-6 A (closed aperture) both NLA and NLR are present in same measurement. B (open aperture) C Pure nonlinear refraction signal by dividing closed aperture one with open aperture.

1-3 Organization of this thesis

In chapter 2, we will introduce theory of Z-scan and derive nonlinear refraction, nonlinear absorption fitting equation. Our Z-scan set-up and sample will be presented in chapter 3. The experimental results of InN and Au nanoparticles are separately presented in chapter 4 and chapter 5. Finally, conclusions and perspective are given in Chapter 6.

Chapter 2 Theoretical background

2-1 Nonlinear refraction

In considering only third order nonlinearity, the refractive can be expressed as equation (1-1). Assuming a TEM_{00} Gaussian beam propagating in +z direction can be written as

$$E(z,r,t) = E_0(t)\frac{w_0}{w}\cdot\exp(-\frac{r^2}{w^2(z)}-\frac{ikr^2}{2R(z)})e^{-i\varphi(z,t)} \qquad (2\text{-}1)$$

where k is wavenumber of the light wave of wavelength λ, $w^2(z) = w_0^2(1+z_0^2/z^2)$ is the beam radius and $R(z) = z(1+z_0^2/z^2)$ is radius of curvature of wavefront at z. $E_0(t)$ denotes the electric field at the focus and contains temporal envelope of laser pulse. $e^{-i\varphi(z,t)}$ is variation of phase that do not depend on r. If the sample is thin enough, the changes in beam diameter within the sample due to diffraction or nonlinear refraction can be neglected. This indicates the sample length L should satisfy a criterion : $L \ll z_0$. With satisfaction of above criterion and using the slowly varied envelope approximation (SVEA), a pair of simple equations can be obtained :

$$\frac{d\Delta\varphi}{dz'} = \Delta n(I)k \qquad (2\text{-}2)$$

and

$$\frac{dI}{dz'} = -\alpha(I)I \qquad (2\text{-}3)$$

where z' is the propagation depth in the sample and α(I), for simplicity, we only consider the linear absorption $\alpha(I) = \alpha_0$. (Next section will discuss nonlinear absorption term, we only consider nonlinear refraction effect here) Solving equation (2-2) and (2-3), phase shift $\Delta\varphi$ at exit surface of sample can be expressed

$$\Delta\varphi(z,r,t) = \Delta\varphi_0(z,t)\exp(-\frac{2r^2}{w^2(z)}) \qquad (2\text{-}4)$$

with

$$\Delta\varphi_0(z,t) = \frac{\Delta\Phi_0(t)}{1+z^2/z_0^2}. \quad (2\text{-}5)$$

$\Delta\Phi_0(t)$ is the on-axis phase shift at the focus:

$$\Delta\Phi_0(t) = k\Delta n L_{eff} \quad (2\text{-}6)$$

and

$$\Delta n = n_2 I_0(t) \quad (2\text{-}7)$$

with effective length $L_{eff} = (1 - e^{-\alpha_0 L})/\alpha_0$ and $I_0(t)$ denotes on-axis irradiance at focus. The electric field exiting the sample with nonlinear phase distortion is then

$$E_e(r,z,t) = E(r,z,t)e^{-\alpha_0 L/2}e^{i\Delta\varphi(z,r,t)} \quad . \quad (2\text{-}8)$$

By using "Gaussian decomposition" (GD) method, the nonlinear phase term $e^{i\Delta\varphi(z,r,t)}$ of electric field at the exit plane of the sample can be decomposed into Taylor series expansion:

$$e^{i\Delta\varphi(z,r,t)} = \sum_{m=0}^{\infty} \frac{[i\Delta\varphi_0(z,t)]^m}{m!} e^{-2mr^2/w^2(z)} \quad (2\text{-}9)$$

Each Gaussian beam cab be propagated to the far field and resumed to reconstruct the beam. We derive the electric field at the aperture:

$$E_a(r,t) = E(z,r=0,t)e^{-\alpha L/2}\sum_{m=0}^{\infty} \frac{[i=\varphi_0(z,t)]^m}{m!}\frac{w_{m0}}{w_m}\cdot\exp(e\frac{r^2}{w_m^2} - \frac{ikr^2}{2R_m} + i\theta_m) \quad (2\text{-}10)$$

where

$$w_{m0}^2 = \frac{w^2(z)}{2m+1},\ d_m = \frac{kw_{m0}^2}{2},$$

$$w_m^2 = w_{m0}^2[g^2 + \frac{d^2}{d_m^2}],\ R_m = [1\ \frac{g}{g^2+d^2/d_m^2}]^{-1},$$

$$\theta_m = \tan^{-1}[\frac{d/d_m}{g}] \text{ and } g=1+d/R(z)$$

The transmitted power through the aperture is obtained by spatially integrating $E_a(r,t)$ up to the aperture radius r_a:

$$P_T\left(\Delta\Phi_0(t)\right) = c\varepsilon_0 n_0 \pi \int_0^{r_a} |E_a(r,t)|^2 \, r dr \qquad (2\text{-}11)$$

And the normalized Z-scan transmittance T(z) can be calculated as

$$T(z) \frac{\int_{-\infty}^{\infty} P_T(\Delta\Phi_0(t))dt}{s\int_{-\infty}^{\infty} P_i(t)dt} \qquad (2\text{-}12)$$

where $P_i(t) = \pi w_0^2 I_0(t)/2$ is instantaneous input power and S=1-exp$(-2r_a^2/w_a^2)$ is linear aperture transmittance, w_a denotes the beam radius at the aperture.

We can simplify this equation, if experiment can satisfy two assumptions. First, nonlinear phase change is small ($|\Delta\Phi_0| \ll 1$). The second is the far field condition ($d \gg z_0$). In this case, approximated expression of on-axis transmittance through aperture can be written:

$$T(z, \Delta\Phi_0) \cong 1 - \frac{4\Delta\Phi_0 x}{(x^2+9)(x^2+1)} \qquad (2\text{-}13)$$

where $x=z/z_0$. Eq.(2-13) is nonlinear refraction fitting formula. By solving the equation $\frac{dT(z,\Delta\Phi_0)}{dz} = 0$, it is interesting to note that the peak-to-valley(or valley-to-peak) separation in z is given by

$$\Delta z_{p-v} = 1.7 z_0$$

And relation between laser depth-of-focus z_0 and beam waist w_0 is given by:

$$z_0 = \frac{\pi w_0^2}{\lambda} \qquad (2\text{-}14)$$

This implies that Δz_{p-v} is only related to the parameters of laser. By measuring laser beam waist w_0, we get z_0 in eq.$(2-14)$. And we set z_0 and $\Delta\Phi_0$ as fitting parameters at the same time when fitting close-aperture Z-scan data by eq.(2-13).

2-2 Nonlinear absorption

If we remove the aperture, the detector would receive all of energy of the beam. The only effect that can contribute to variation in transmittance is the nonlinear absorption. In this case, $\alpha(I)$ in equation (2-3) should include a nonlinear absorption term:

$$\alpha(I) = \alpha_0 + \beta I$$

where β is nonlinear absorption coefficient. By solving equation (2-2) and (2-3), the phase shift and intensity as beam exiting the sample can be obtained:

$$\Delta\varphi(z, r, t) = \frac{kn_2}{\beta}\ln[1 + q(z, r, t)] \quad (2\text{-}15)$$

and

$$I_e(z, r, t) = \frac{I(z,r,t)e^{-\alpha L}}{1+q(z,r,t)} \quad (2\text{-}16)$$

Since we are interested in total transmittance, we only have to integrate eq. (2.16) over r without considering the free-space propagation. After this integration, the transmitted power P(z,t) can be shown

$$P(z, t) = P_i(t)e^{-\alpha L}\frac{\ln[1+q_0(z,t)]}{q_0(z,t)} \quad (2\text{-}17)$$

where $q_0(z, t) = \beta I_0(t)L_{eff}/(1 + z^2/z_0^2)$ and $P_i(t)$ is defined in eq.(2-12). For a temporally Gaussian pulse, we integrate eq. (2-17) over time and obtain:

$$T(z) = \frac{1}{\sqrt{\pi}q_0(a,0)} \cdot \int_{-\infty}^{\infty} \ln\left[1 + q_0(z, 0)e^{-\tau^2}\right]d\tau \quad (2\text{-}18)$$

For $|q_0| < 1$, eq. (2-18) can be expressed as series which is more suitable for numerical fitting:

$$T(z) = \sum_{m=0}^{\infty} \frac{[-q_0(z,0)]^m}{(m+1)^{3/2}} \quad (2\text{-}19)$$

We can get nonlinear absorption coefficient by using eq.(2-19) to fit OA Z-scan data.

2-3 Effective fifth-order nonlinearity

If a material presents two-photon absorption, the change in refraction that caused by the free electrons cannot be neglected as we increase optical intensity.[2-1],[2-2] In this case, if two-photon absorption is the only mechanism for generating carrier, eq.(2-2) should be corrected as

$$\Delta n = n_2 I + C\sigma I^2 \quad (2\text{-}20)$$

$$C=0.23(\beta t_0/\hbar\omega) \qquad (2\text{-}21)$$

where n_2 is third-order nonlinear index that is usually due to bound electrons. σ is effective fifth-order nonlinearity which is resulted from two-photon-absorption generated free carrier. From eq. (2-20) , it is clear that electronic Kerr effect (n_2I) will be dominant at low irradiance, however, the free carrier refraction (σI^2) will be dominant at high irradiance. For simplicity of numerical fitting, we usually rewrite eq. (2-20) as

$$\Delta n/I = n_2 + C\sigma I \qquad (2\text{-}22)$$

To separate 3rd-order and 5th-order nonlinear refractive index, we can repeat Z-scan at different irradiance and get phase-shift ($\Delta\Phi_0$) by numerical fitting. Then, we can obtain change in refraction Δn by eq.(2-6) and draw a diagraph of Δn/I vs. I. Then using eq. (2-22), the intercept at Y-axis is n_2 and slope is Cσ, as shown in [figure 2-1] .

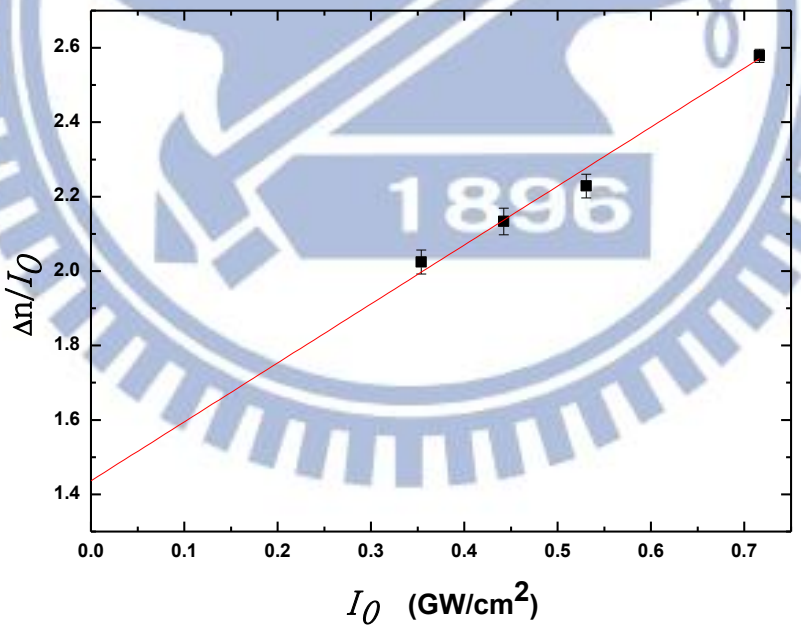

Fig. 2-1 Z-scan result of ZnTe which is excited by 800nm wavelength. The intercept at Y-axis is third-order nonlinearity n_2 and slope is effective fifth-order nonlinearity Cσ.

Chapter 3 Experiments

3-1 Z-scan Experimental Set-up

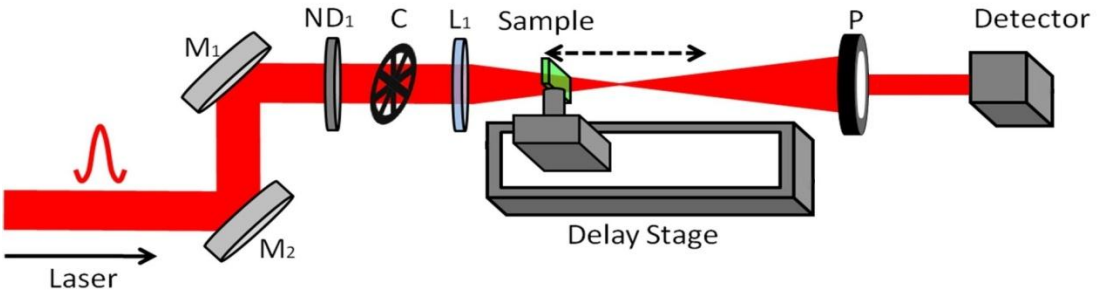

Fig. 3-1 The Z-scan setup. M : mirror, C : chopper, L : focusing lens, P : aperture

Femtosecond laser system

To photoexcite the sample, we used a Ti:sapphire laser amplified by a regenerative amplifier and a home-made fiber laser. And the basic properties of femtosencond system are described below.

Table 1 Properties of Ti-Sapphire laser, regenerative amplifier and fiber laser

	Ti：Sapphire laser (Tsunami, Spectra-Physics)	**Regenerative amplifier (Spitfire, Spectra-Physics)**	**Fiber laser (home-made)**
Wavelength	800 nm	800 nm	1550nm
Pulse Width	35 fs	50 fs	150fs
Repetition Rate	82 MHz	1 kHz	76MHz

The setup of the Z-scan system is shown in Figure 3-1. The laser beam is focused to a sample by a positive lens with a 10 cm focus-length. And the radius of beam waist after focusing is 15μm and 10μm for the MHz and kHz systems, respectively. A

motorized translation stage is used to move the sample along z-axis with the spatial resolution of 10μm. The laser beam was chopped by a chopper at 1 kHz and 400 Hz for the MHz and kHz systems, respectively. In order to increase the signal-to-noise ratio, the transmittance of the beam through the sample was detected by a photodiode and the electric signal was connected to a lock-in amplifier (Stanford Research SR830). Nonlinear refractive index and nonlinear absorption can be determined by close- and open-aperture. Each measurement was repeated 3 times and we used averaged values to plot Z-scan traces. Before starting to measure the Z-scan data of the target material, we used a ZnTe crystal as a reference material to make sure our system is calibrated correctly. We performed both OA and CA measurement at different optical intensity as shown in Figure 3-2. By using eq. (2-19) to fit the OA Z-scan data, we got a nonlinear absorption coefficient $\beta = 14.26\text{cm/GW}$, as depicted in Figure 3-3. We fitted the CA Z-scan data using eq. (2-13) and obtained change in phase $\Delta\Phi_0$. By using eq. (2-6), Δn can be obtained and we plotted Δn/I vs. I graph. Then, fitting by eq. (2-22), we got third-order nonlinear refractive index $n_2=1.436(\pm0.06)\times10^{-13}$from the intercept at Y-axis and fifth-order nonlinearity $\sigma=1.2(\pm0.07)\times10^{-19}$ from the slope Cσ (C is a constant and can be calculated from $C=0.23(\beta t_0/\hbar\omega)$) in Figure 3-4. Note that the errors are fitting errors. Table 2 shows the comparison between the results of previous measurements[3-1] and our results and an excellent agreement can be observed.

Table 2 The nonlinear parameters of ZnTe crystal measured at 800 nm.

	β(cm/GW)	$n_2(\text{cm}^2/\text{W})$	$\sigma(\text{cm}^3)$
Ref.3-1	16.1	1.373×10^{-13}	1.439×10^{-19}
Our results	$14.26(\pm0.8)$	$1.436(\pm0.06)\times10^{-13}$	$1.2(\pm0.07)\times10^{-19}$

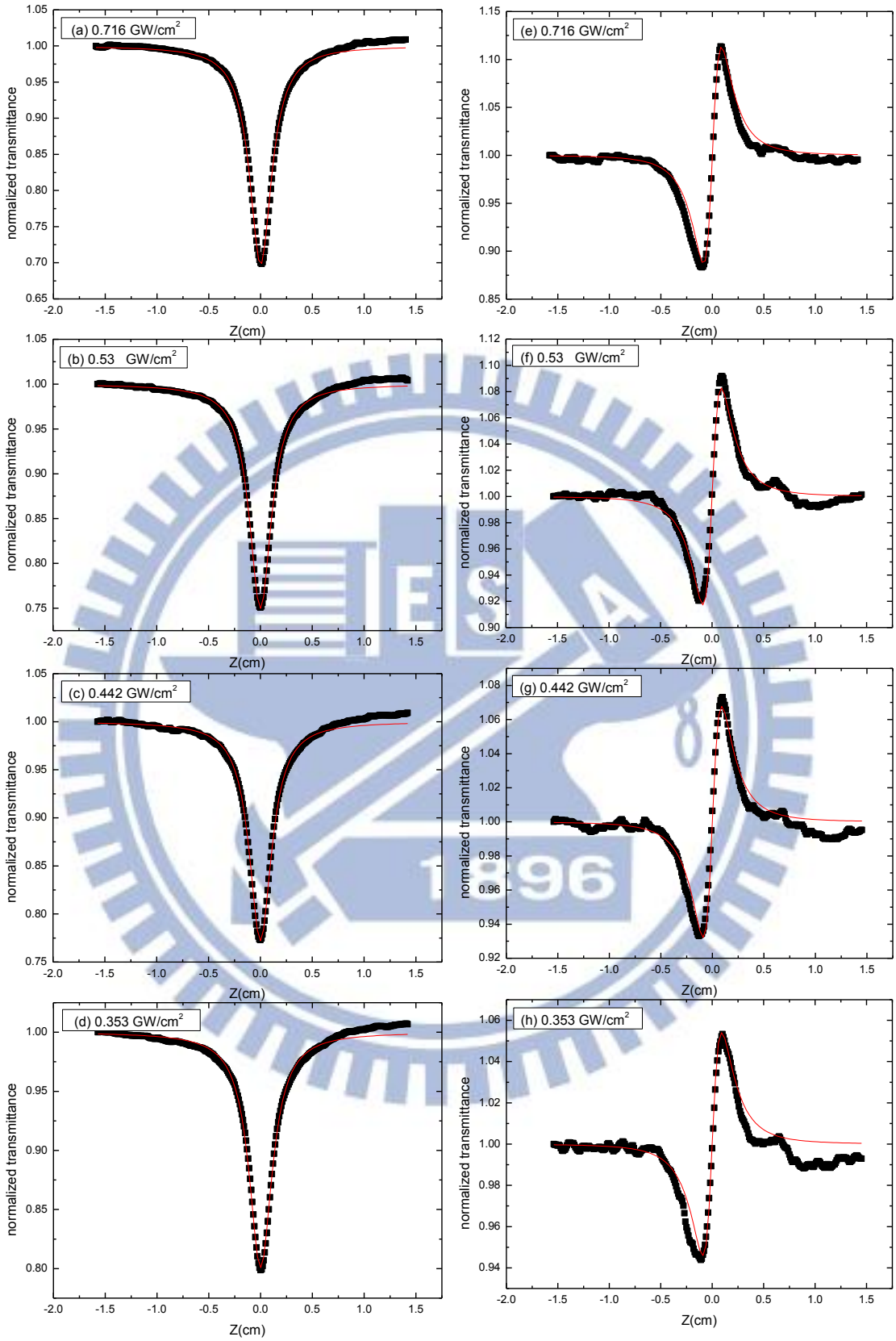

Fig. 3-2 (a),(b),(c),(d) shows ZnTe open-aperture traces. (e),(f),(g),(h) shows ZnTe close-aperture divided by open-aperture traces with different input intensity. The filled squares are experimental data and the solid line are fitting curves.

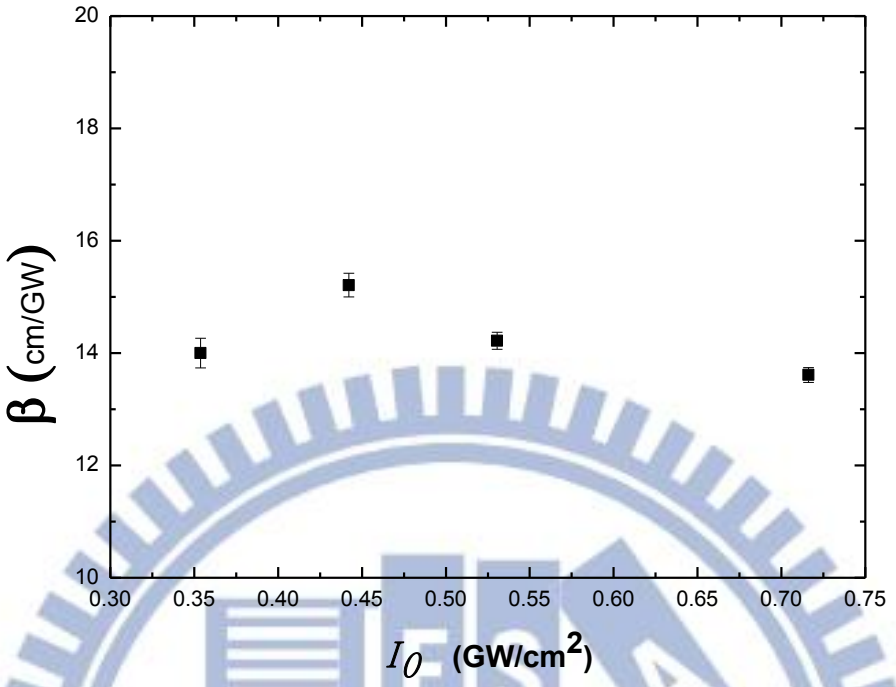

Fig. 3-3 ZnTe two photon absorption coefficient which is plotted with optical intensity shows power-independent.

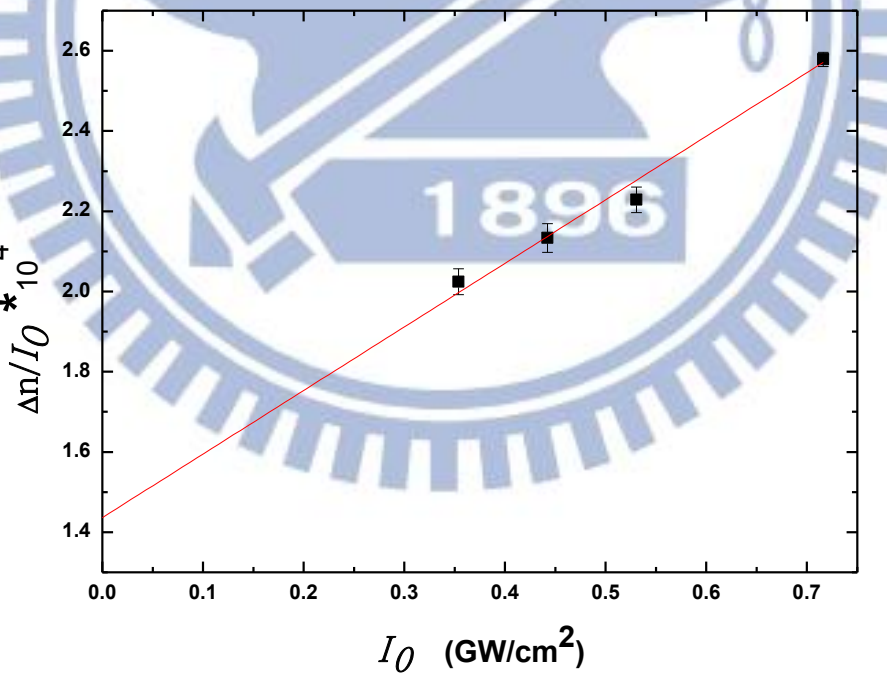

Fig. 3-4 The intercept with Y-axis is n_2 and the slope is concerned with σ.

3-2 Background Subtraction

Samples with surface imperfection or wedge may cause systematic transmittance changes that can mask the nonlinear refraction signal, as shown in Figure 3-5. To reduce this effect, we can do low irradiance (low enough that nonlinear signal is negligible) Z-scan and let high irradiance data subtract low irradiance data after normalizing each scan. Figure 3-6 illustrates the procedure described above.

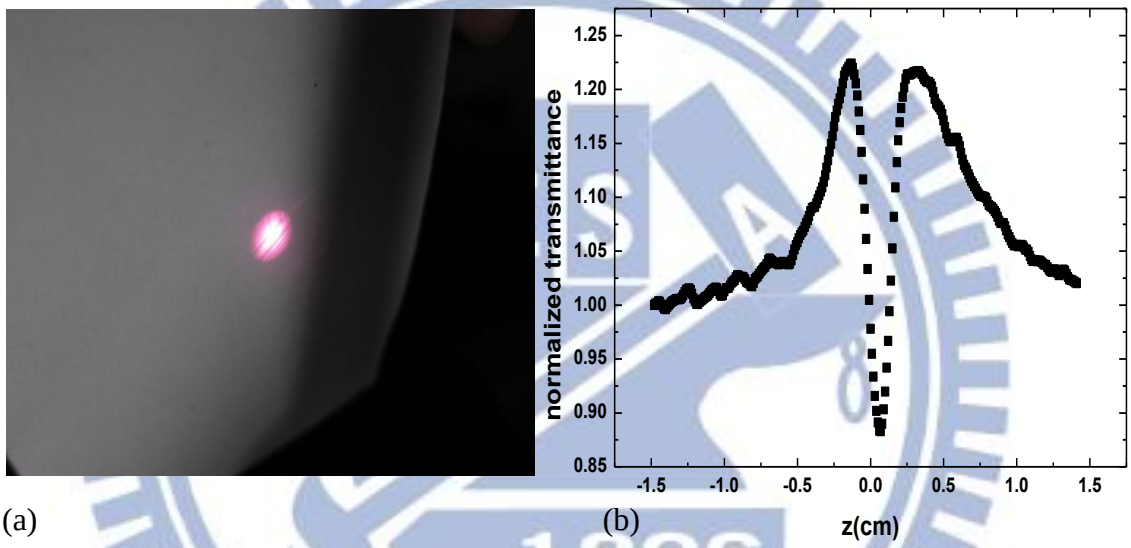

(a) (b)

Fig. 3-5 (a) The beam profile is seriously destroyed after going through a sample with poor surface quality. (b) The low irradiance Z-scan measurement showed background and this change of transmittance is so big that can totally block out the sample's nonlinear signal.

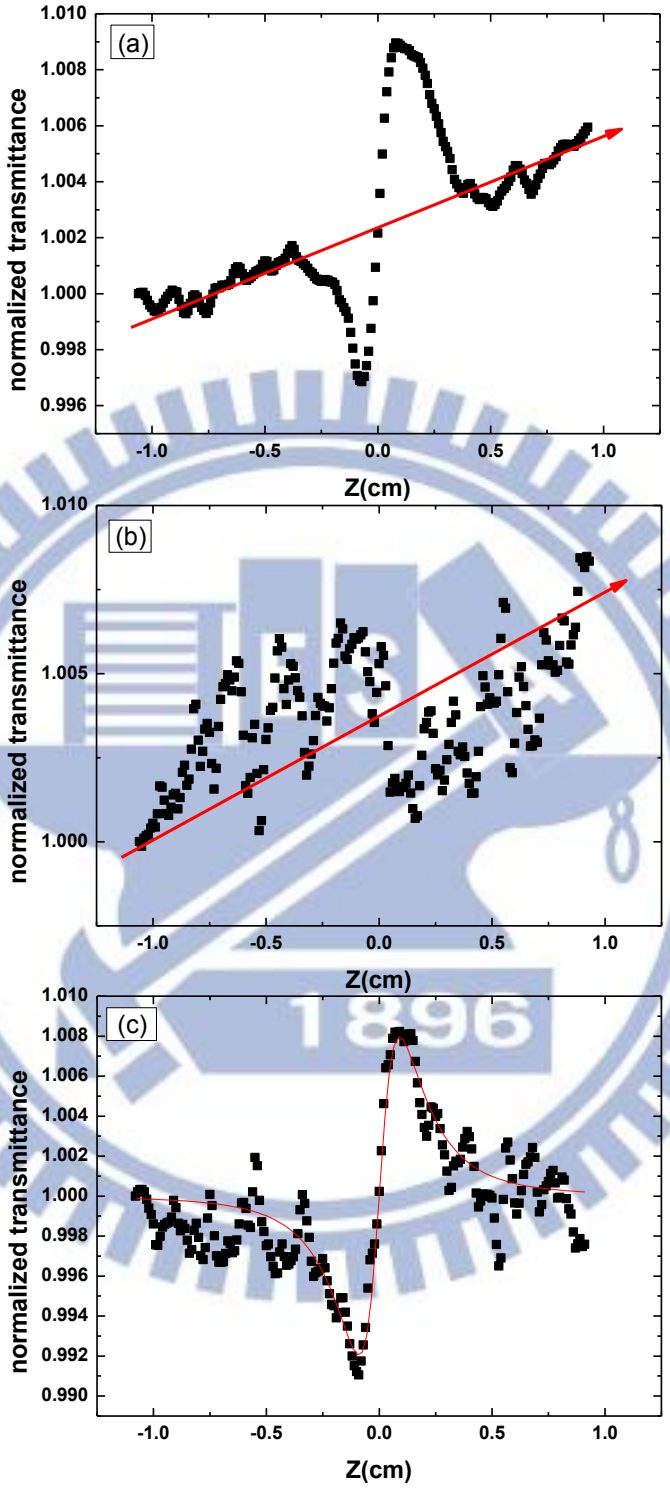

Fig. 3-6 (a) the nonlinear refractive signal is probably caused by sample's surface wedge, so the Z-scan traces are not symmetrical. (b) The low irradiance Z-scan at same point which shows the effect of surface wedge. (c) Net transmittance change versus Z after the background subtraction, the solid line is fitting curve.

3-3 Au nanoparticles

The Au nanoparticle supercrystals were synthesized using layer-by-layer assembly from suspensions of octadecanethiolate-passivated Au colloids. Au nanoparticles floating on the top of oversaturated solution were transferred to any chosen substrate consecutively by dipping the substrate and pulling it out perpendicular to the liquid surface. This assembly method is called “dip coating” which can be applied to any chosen substrate [quartz, indium tin oxide (ITO), silicon, or gold]. The core of Au nanoparticle is ~6 nm and the in-plane lattice constant of monolayer is ~9 nm. Figure 3-7 shows the field-emission scanning electron microscopy (FE-SEM) images. The reflectance spectra from these supercrystal films show that plasmonic transverse (T-mode) and longitudinal modes(L-mode) can be observed as layer number is larger than 10 monolayers. In Fig. 3-8, reflectance spectra from these supercrytal films are different from a sputtered gold film. The presence of reflectance peak fixed at 568nm which is caused by T-mode will be clear as layer number is larger than 10 monolayer. However, clear reflectance dips (marked by order number m=1) start to appear and shift to longer wavelength as increasing layer number, which was not observed in the measurement of gold film (gold film spectrum is flat as shown in Fig. 3-8). In the subsequent spectra, another reflectance dips (m=2) show up and L-mode can be identified. In contrast to T-mode, the reflectance peak due to L-mode depends on layer number and shift into near-IR region of spectrum as increasing layer number. We expected large nonlinearities caused by L-mode and prepared Au nanoparticle films (on quartz substrate) with 1-, 2-, 3-, 5-, 10-monolayers to investigate the nonlinear refractive index and nonlinear absorption by using Z-scan.

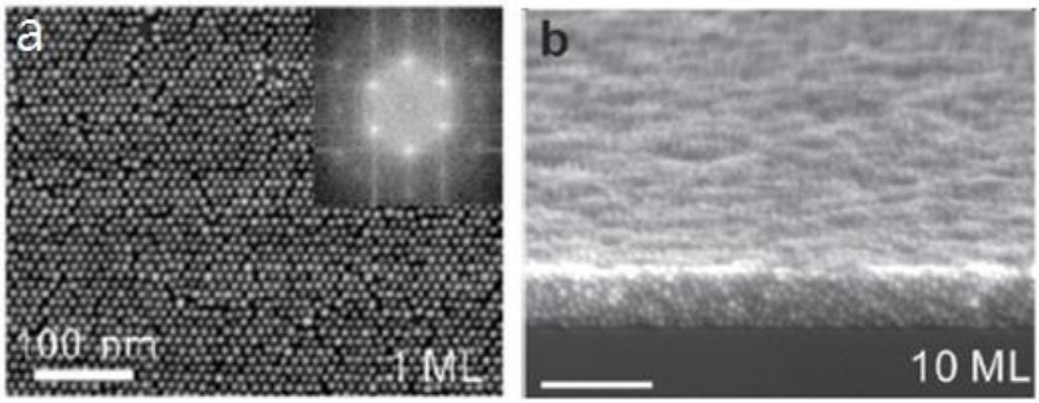

Fig.3-7 (a) FE-SEM image of the first nanoparticle monolayer and (b) cross-sectional image of a 10-monolayer Au nanoparticle film.[1-4]

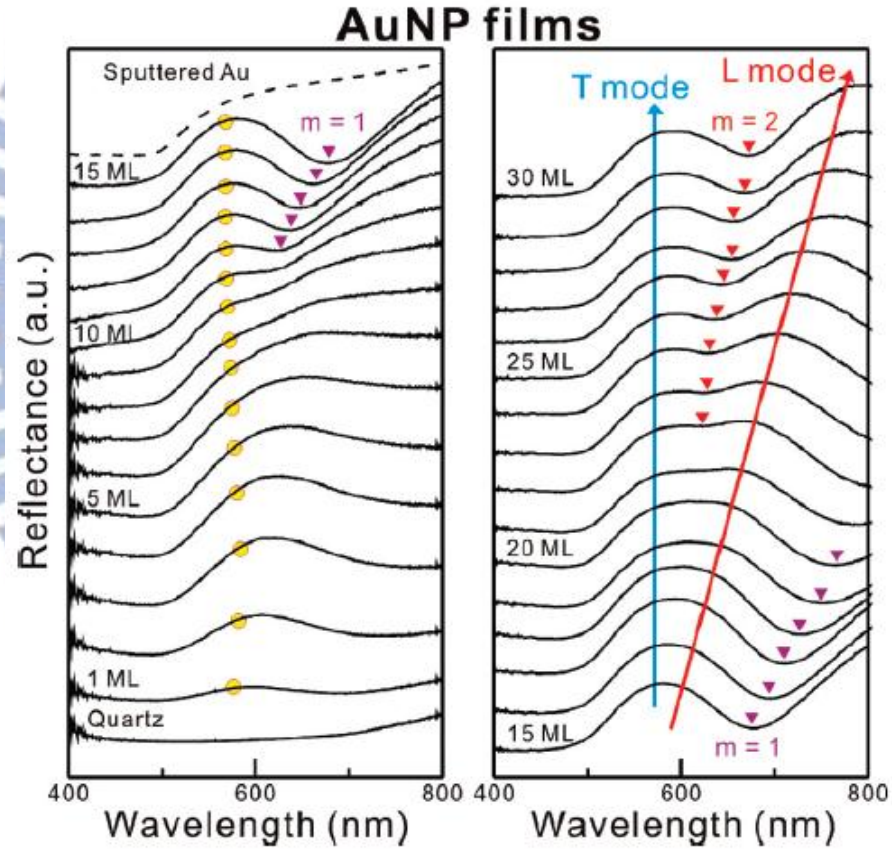

Fig.3-8 Reflectance measurements at normal incidence for Au nanoparticle film on quartz substrate. After 10-monolayer, reflectance peak of T-mode fixed at 568nm and m=1 reflectance dip begin to appear. Both T-mode and L-mode can be clearly identified from 15- to 30-monolayer. Furthermore, L-mode shows the layer-dependence.[1-4]

Table3 Thickness of 3D Au nanoparticle supercrystal

	1-Layer	2-Layer	3-Layer	5-Layer	10-Layer
L (Thickness)	10nm	15nm	20nm	30nm	55nm

3-4 InN thin film

For this work, an a-plane InN epitaxial film is provided by Prof. Gwo's lab in National Tsing Hua University. InN film with the thickness of 50 nm was grown on r-plane sapphire substrates by plasma-assisted molecular-beam epitaxy (PA-MBE). There are two buffer layers which are a-plane AlN (300nm) and a-plane GaN (300nm) between r-plane sapphire and InN thin film.

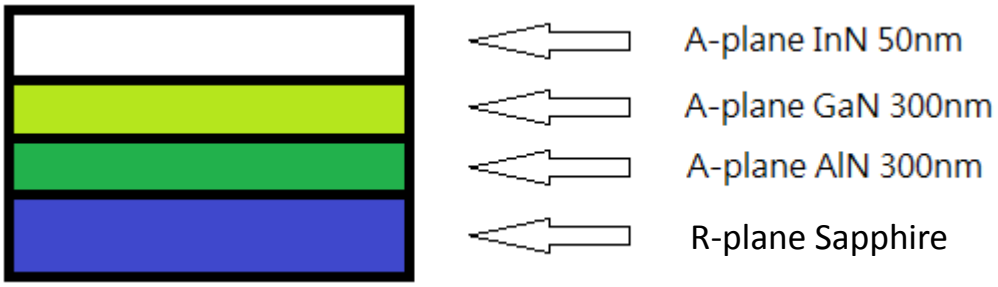

Chapter 4 Z-scan measurement of InN film

We performed the Z-scan measurement of InN thin film at wavelength 800 nm and 1550 nm. The Z-scan traces of OA and CA measured at 800 nm and 1550 nm are separately shown in Fig. 4-1 and Fig. 4-2. In order to make sure there is no contribution from the substrate (GaN 300nm, AlN300nm, sapphire), we repeated the same measurement on the substrate. As shown in Fig. 4-3, no signal was found in both wavelengths. Previous Z-scan result of the InN film in Figure 4-4 shows that there is no nonlinear absorption and the nonlinear refractive index is negative at wavelength 800 nm. We use eq. (2-19) to fit InN OA Z-scan traces and get nonlinear absorption β. For calculating $\mathbf{n_2}$, we set $\Delta\boldsymbol{\Phi_0}$, Z_0 as fitting parameters and use eq. (2-13) to fit CA Z-scan traces. Then $\mathbf{n_2}$ can be calculated from $\Delta\boldsymbol{\Phi_0(t) = kn_2 I_0 L_{eff}}$, where effective length $L_{eff}=(1-e^{-\alpha L})/\alpha$ can be calculated as L_{eff}=40nm at wavelength 800nm, L_{eff}=47nm at wavelength 1550nm. The CA fitting results are listed in Table 4. The results of the Z-scan measurement can be affected by the high repetition rate of the laser source, which induces local thermal effects in the sample during the measurement. With the strong thermal effect, the sample behaves like an optical lens which may lead to an overestimation of nonlinear parameters obtained by the Z-scan method. The thermal contribution to the measured change in the refractive index, can be estimated by calculating the average on-axis refractive index change at focus given by[4-2],

$$\Delta n_0 \cong \frac{dn}{dT}\frac{0.5F_0\alpha}{\rho C_v}$$

where $\frac{\mathbf{dn}}{\mathbf{dT}}$ is thermal optical coefficient, F_0 is the flounce at focus point, ρ is the density, Cv is the specific heat, α is absorption coefficient. F_0 in our experiment is calculated $\mathbf{1.035 \times 10^{-4}\ J/cm^2}$. InN density ρ is 6.1 g/cm^3 [4-3], specific heat is

0.31 J/g.K [4-3], linear absorption coefficient α of InN is $\mathbf{8.7 \times 10^4\ cm^{-1}}$ at 790nm[4-4]. Thermal optical coefficient of InN is estimated to be ~$\mathbf{10^{-4}\ K^{-1}}$ [4-5],[4-6]. And the change in refractive index caused by thermal effect can be estimated to be $\mathbf{\Delta n_0 = 2.4 \times 10^{-4}}$. Compared with the value $\mathbf{\Delta n = n_2 I = 0.12}$ obtained from the fitting of Fig. 4-1, the contribution of thermal effect is negligibly small. The same process was done at wavelength 1550nm and thermal effect also can be neglected too. The comparison between our experimental results and thermal effect is listed in Table 5.The nonlinear absorption coefficient of InN measured by Tsai et al.[4-7] at different repetition rates is consistent with our result of $\mathbf{\Delta n}$. Our results measured at 800 nm shows the absorption saturation ($\mathbf{\beta<0}$) and self-focusing ($\mathbf{n_2 > 0}$), while at 1550nm the results shows reverse saturable absorption ($\mathbf{\beta>0}$) and self-focus ($\mathbf{n_2 > 0}$). The numbers of β and $\mathbf{n_2}$ are listed in Table 6. The listed errors in Table 6 are fitting errors. And β is power-independent as shown figure 4-5, figure 4-6.

Table 4 CA Z-scan traces fitting results.

Wavelength(nm)	$\mathbf{\Delta\Phi_0}$	Z_0 (cm)	n_2 (cm^2/W)
800	0.038	0.11	$(5.84) \times 10^{-11}$
1550	0.0183	0.27	$(1.86) \times 10^{-10}$

Table 5 Comparison between our experimental results and thermal effect.

Wavelength(nm)	$\Delta n = n_2 I$(from our experimental data)	Δn_0(thermal effect contribution)
800	0.12	2.4×10^{-4}
1550	0.096	9.1×10^{-5}

Table 6 Nonlinear optical parameters of InN film

Wavelength(nm)	β(cm/W)	$n_2(cm^2/W)$
800	$-(2.12 \pm 0.06) \times 10^{-6}$	$(5.84 \pm 0.2) \times 10^{-11}$
1550	$(1.65 \pm 0.01) \times 10^{-5}$	$(1.86 \pm 0.1) \times 10^{-10}$

The saturable absorption behavior of the InN sample can be explained by the band filling effect. When an InN sample is irradiated by a laser pulse with a wavelength of 800 nm, free carriers are generated through the linear absorption. As the photon-induced free carriers occupy the conduction band, they prevent more electrons from entering to the conduction band and lead to the reduction of absorption. The direct interband absorption coefficient at energy $\hbar\omega$ can be written as[4-8]

$$\Delta\alpha(\hbar\omega) = -\frac{16\pi^{3/2}}{3}\frac{e^2\hbar}{m_v}\left(\frac{\mu}{m_v}\right)^{3/2}\frac{1}{n_0}\frac{m_e P^2}{\hbar^2}\frac{(\hbar\omega - E_g)^{1/2}}{\hbar\omega}\frac{\Delta N}{(k_B T)^{3/2}}\exp\left[\frac{-\mu(\hbar\omega - E_g)}{m_v k_B T}\right]$$

where $\mu = m_c m_v/(m_c+m_v)$ is the reduced mass (m_c and m_v are the conduction- and valence-band effective masses, respectively) and $P = -(i\hbar/m_e)\langle S|p_z|Z\rangle$ momentum matrix element. m_e is the static electron mass and n_0 and E_g are the linear refractive index and the band gap, respectively. ΔN is the photoexcited free electron density. This equation shows that the laser-induced absorption coefficient change Δα ($=\alpha - \alpha_0=\beta\times I_0$) is negative ($\beta < 0$), which means that higher laser intensity leads to lower absorption and results in higher transmission. It is consistent with our results at 800nm.

The increase of absorption in the Z-scan measurement can be often observed for the photoexcitation below the bandgap energy through the reverse saturation absorption attribute to two-photon absorption. Since the photon energy of 1550 nm laser pulses is

larger than the bandgap energy of InN, the reverse saturation absorption due to two-photon absorption can be excluded for our experiment. Meanwhile, when the carrier density photogenerated during the Z-scan measurement is high, the carrier screening of the internal electric field may occur near the bottom of the conduction band. The injected electrons will occupy states at the bottom of the conduction band. If the electron concentration is large enough, the electron wave function will overlap, forming a gas of interacting particles. The electrons will repel one another by Coulomb forces. In addition, electrons with the same spin will avoid one another for statistical reasons. The net result is a screening of electrons and a decrease in their energy, lowering the energy of the conduction band edge. Band-gap renormalization usually dominate at high photoexcited carrier density N which can be obtained by the relation of,

$$N = \frac{(1-R)F\alpha}{\hbar\omega}$$

where α is linear absorption coefficient, R is reflectivity, F is irradiance at focus. $\alpha = 2.23 \times 10^4 \mathrm{cm}^{-1}$, R=25%, F= $7.73 \times 10^{-5}\ \mathrm{J/cm^2}$, this is properties of InN measured at 1550nm, photoexcited free electron density can be calculated N=$1.01 \times 10^{19}\ \mathrm{cm}^{-3}$. The ultrafast carrier relaxation time of InN is in the range of picosecond and at 1550 nm, InN displays close to resonant behavior. Highly photoexcited carriers quickly gather near the bottom of the conduction band as they cool down and the significant carrier screening can be observed at 1550 nm. Therefore, the nonlinear absorption at 1550nm may be caused by band-gap renormalization.

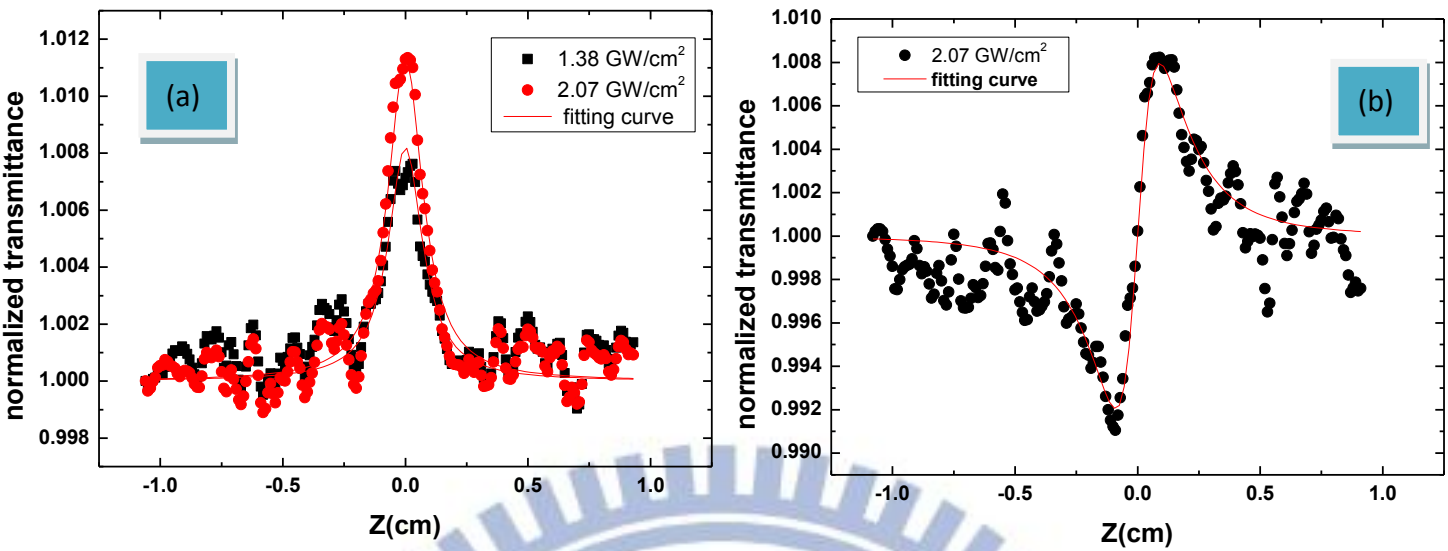

Fig. 4-1 (a) Open-aperture Z-scan traces at 800nm. (b) Close-aperture Z-scan traces at 800nm.

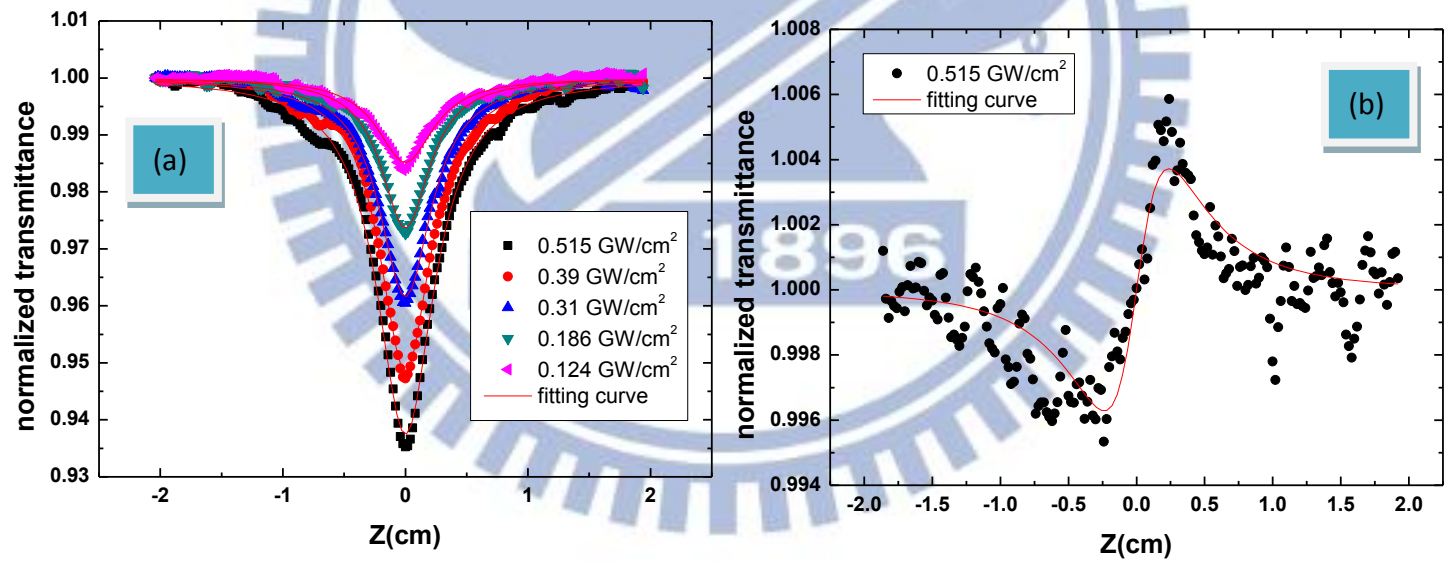

Fig. 4-2 (a) Open-aperture Z-scan traces at 1550nm. (b) Close-aperture Z-scan traces at 1550nm.

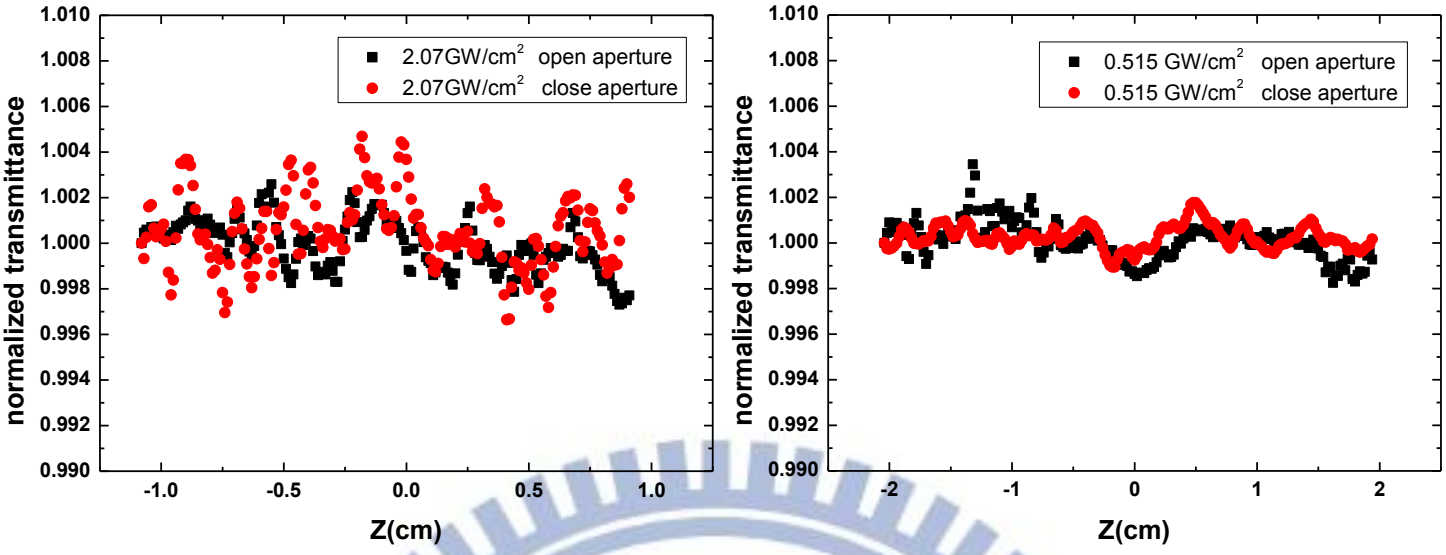

Fig. 4-3 (a) Z-scan traces of substrate at 800nm. (b) Z-scan traces of substrate at 1550nm.

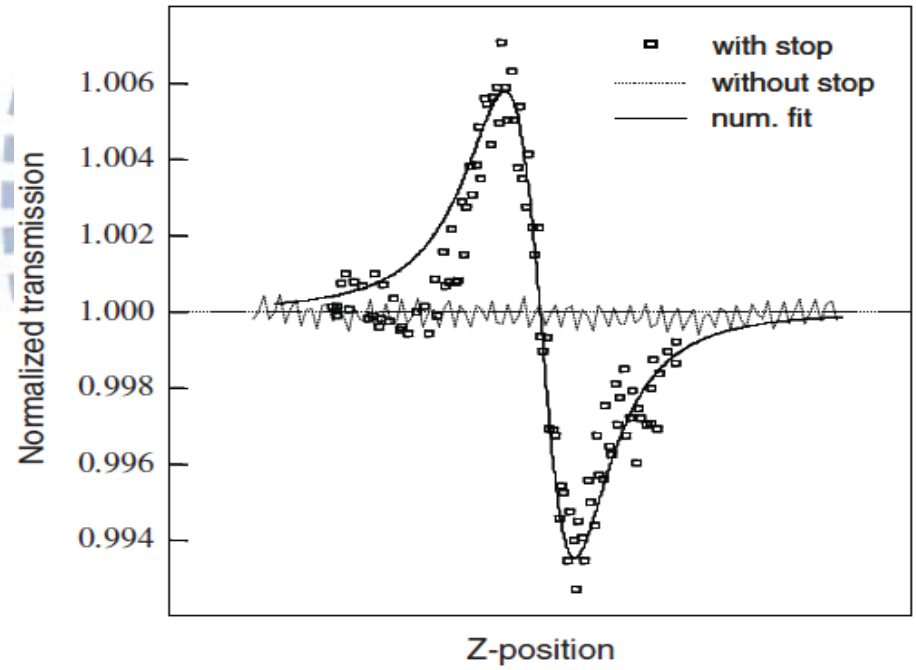

Fig. 4-4 Z-scan Measurement of GaN thin films at 800 nm.[4-1] Hollow-square is close-aperture Z-scan traces which indicates self-defocus ($n_2<0$). Our close-aperture Z-scan traces in [Fig. 4-1] and [Fig. 4-2] which indicate self-focus ($n_2>0$) is opposite to this results, so nonlinear effect of GaN is negligible in our measurement. The number of $n_2=-7.3\times10^{-14}$ reported from reference 4-1. The noise of our measurement is too large so we can't observe nonlinearity of GaN in [Fig. 4-3].

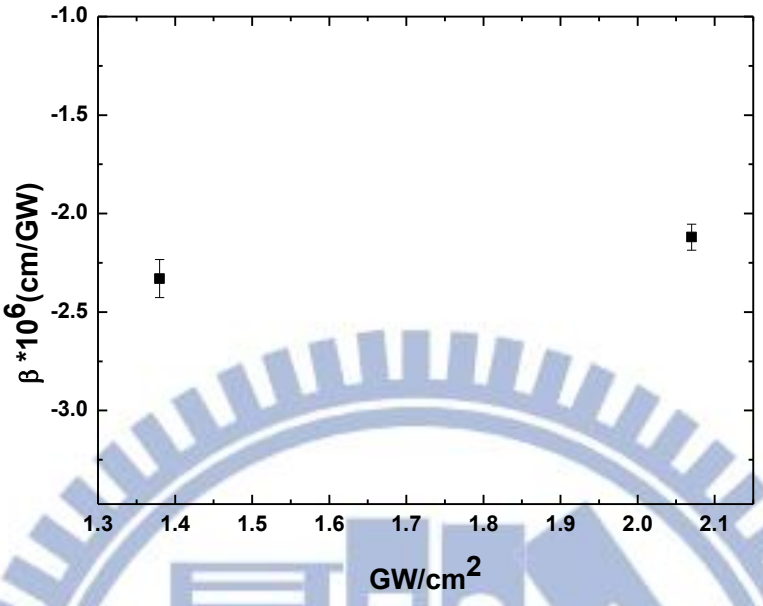

Fig. 4-5 InN nonlinear absorption coefficient at 800nm.

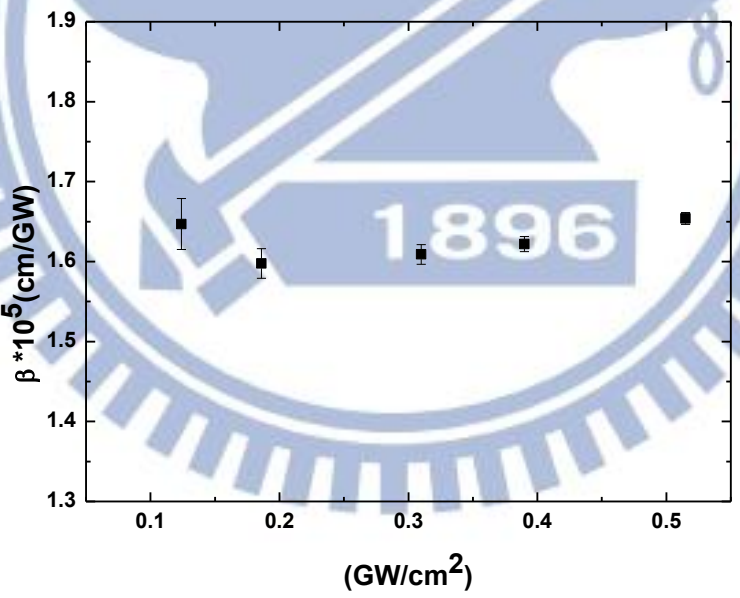

Fig. 4-6 InN nonlinear absorption coefficient at 1550nm which is plotted with optical intensity shows power-independent.

Chapter 5 Results of 3D Au nanoparticle supercrystal

According to Fig. 3-8, the L-mode of Au nanoparticle supercrystal has a resonance at near 800 nm and its effect gets stronger as the layer number increases. By employing the Z-scan method, we investigated the nonlinear properties of Au nanoparticle supercrystal. Up to now the optical properties of 2D Au nanostructures has been intensely studied mainly due to the difficulty of fabrication of 3D structures. We measured the nonlinear coefficients of Au nanoparticles as a function of layer number and laser fluence. We found that the thermal effect which prevents the accurate determination of the nonlinear properties of material by the Z-scan method is exceptionally strong for Au nanoparticls. In this chapter, we present the results of the Z-scan measurement excited by two lasers with the repetition rate of 80 MHz and 1 kHz, respectively.

5-1 The results of Z-scan with an 80MHz laser : Thermal-lens effect

We performed the Z-scan measurement on Au nanoparticles with a Ti:sapphire laser with the repetition rate of 80MHz. The Z-scan signal from thin Au film at 800 nm is too small to be detected in our measurement system. However, Figs. 5-1 and 5-2 show that the Z-scan signals from Au nanoparticle measured in both CA ad OA configurations are very large even with the optical intensity of just several hundreds of $\mathrm{MW/cm^2}$. And the calculated nonlinear refractive index χ^3 was in the order of 10^{-5} to 10^{-3}. Furthemore, we observed the OA Z-scan signals changing sign and getting larger as the excitation time increases when using low optical intensity, Figs. 5-3. We attributed the observed abnormally large χ^3 to "thermal-lens effect".[5-1] The thermal-lens effect and Kerr effect are both related to laser spatial Gaussian profile. But the thermal-lens effect is caused by the temperature dependence of refractive index n_0. When the refractive index is temperature dependent $(\mathrm{dn/dT} \neq 0)$, a

formation of lens can be created at the photoexcited region and cause the beam divergence in the Z-scan experiment. There are two conditions of laser that thermal effect becomes significant.[5-2] First is the long laser pulsewidth. The characteristic time of electron-phonon coupling is estimated to be 50-200 ps.[5-3] Therefore, the Z-scan measurement of Au samples with the pulses longer than 200 ps can lead to the serious thermal effect. Since a femtosecond laser is used in our Z-scan experiment, we can exclude this situation. Second, high repetition rate causes cumulative thermal effect. If laser pulse spacing is shorter than characteristic thermal-diffusion time t_c, the sample will not return to equilibrium temperature within the time interval between consecutive pulses. Instead, it will cause cumulative heating in excited region and once heat absorbed in the excited region of sample and heat diffused to all direction become equilibrium, a quasi-permanent spatial temperature distribution is created: the excited region of sample is hotter on the beam axis and the temperature decreases along radius. Due to the refractive index dependence on temperature, a thermal-lens is then created at the center of excited area and produces the transmittance change in the CA Z-scan singals. The characteristic thermal-diffusion time t_c is a critical parameter that can be written as [5-4], [5-5]:

$$t_c = \frac{\omega^2 \rho c_p}{4\kappa}$$

where ω is the laser spot size and ρ is density, c_p is specific heat, κ is thermal conductivity. For Au, $\rho = 19.3(g/cm^3)$, $c_p = 0.126(Jg^{-1}K^{-1})$, $\kappa = 318(Wm^{-1}K^{-1})$ and beam waist in our experiment is 15μm, t_c can be estimated $t_c \sim 0.2$ μs, which is much longer than period of our laser pulses about 12.2 ns. Thus the above condition can be met and thermal-lens effect would play an important role when we used MHz laser. In fact, the thermal effect was so strong that can damage our sample. Figure 5-4 shows, the morphology of the excited area observed by an SEM. The excited area has

the morphology of molten gold which is quickly resolidified. Open-aperture Z-scan traces for multilayers show the increase of absorption, as shown in Figure 5-2. This can be described by the photodarkening effect[5-6]. For monolayer sample, the Z-scan traces for OA and CA have the opposite sign to the traces of multilayers. For multilayers, the peak-valley CA traces indicate that the thermal-lens effect makes the sample act like a negative lens. It also implies that our Au nanoparticle's refractive index decrease as temperature increases $(dn/dT < 0)$. In contrast, monolayer of Au nanoparticles tends to act like a positive lens as shown in the inset of Figure 5-1. We measured the Z-scan trace of quartz substrate and found that there is no nonlinear signal.

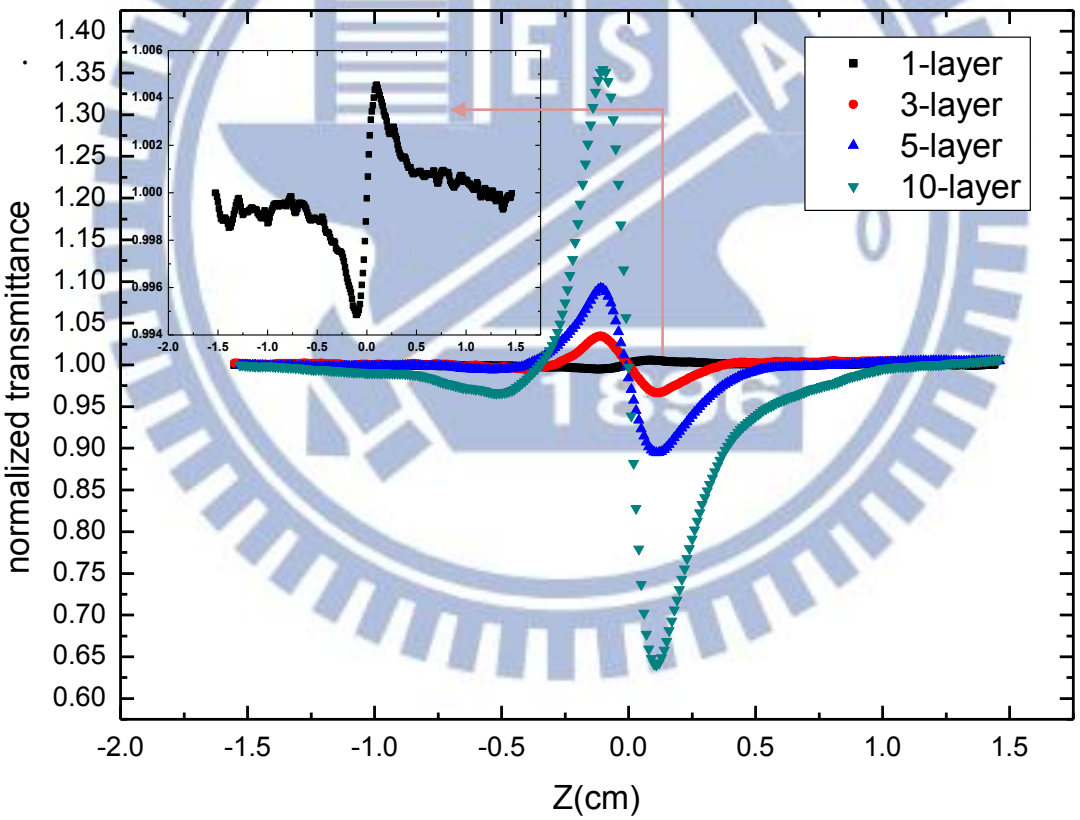

Fig. 5-1 The different Au nanoparticle layer close-aperture Z-scan trace which is excited at 0.4 GW/cm^2. The inset in the figure shows that 1-layer tends to focus beam. It is different from other layers.

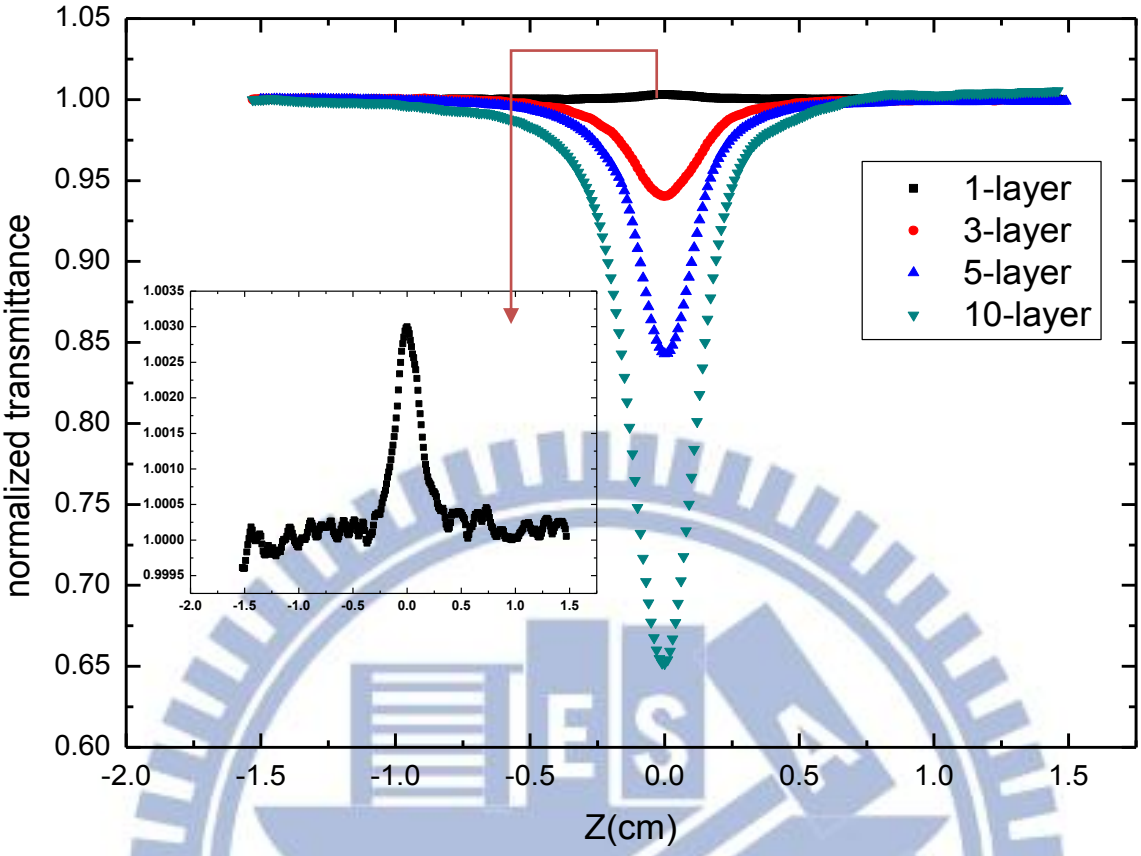

Fig. 5-2 The different Au nanoparticle layer open-aperture Z-scan trace which is excited at 0.4 GW/cm^2 .

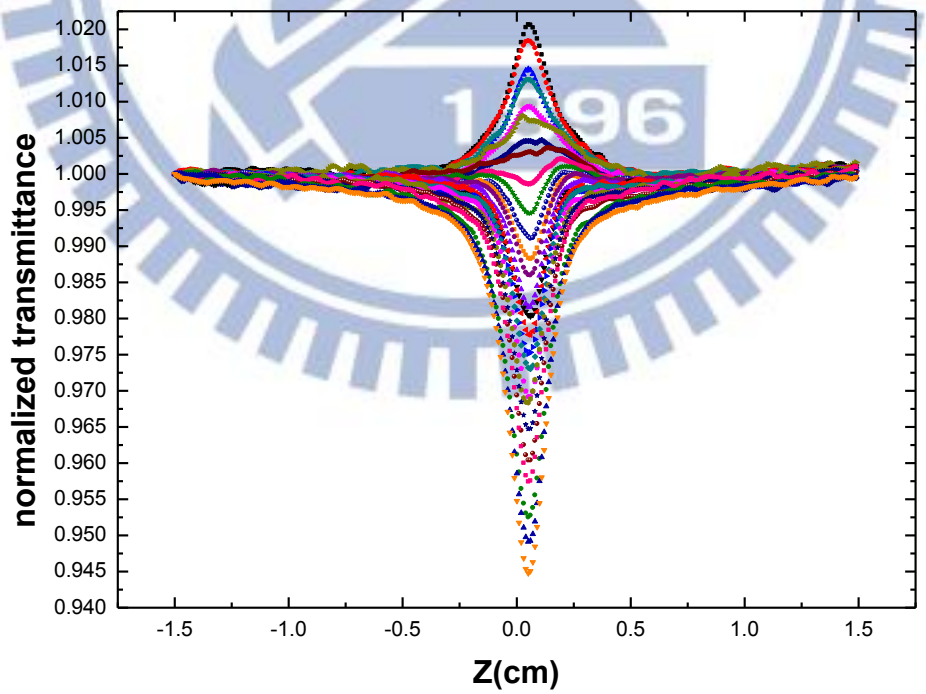

Fig. 5-3 Continually excited 10-layers Au nanoparticle with 82 MHz laser 2 hours.

Transmittance changed from satruation absorption to increase absorption.

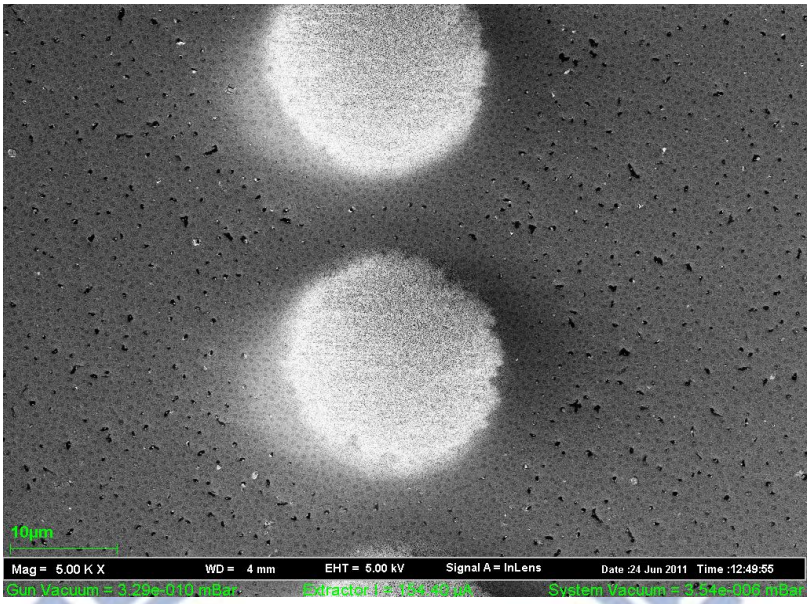

Fig. 5-4 (a)Using the 80MHz laser to make pattern on the 5-layers nanoparticles. It shows the difference compared with results of 1KHz. This patter is excited at 0.8GW/cm^2 and exposure time is 5 minutes.

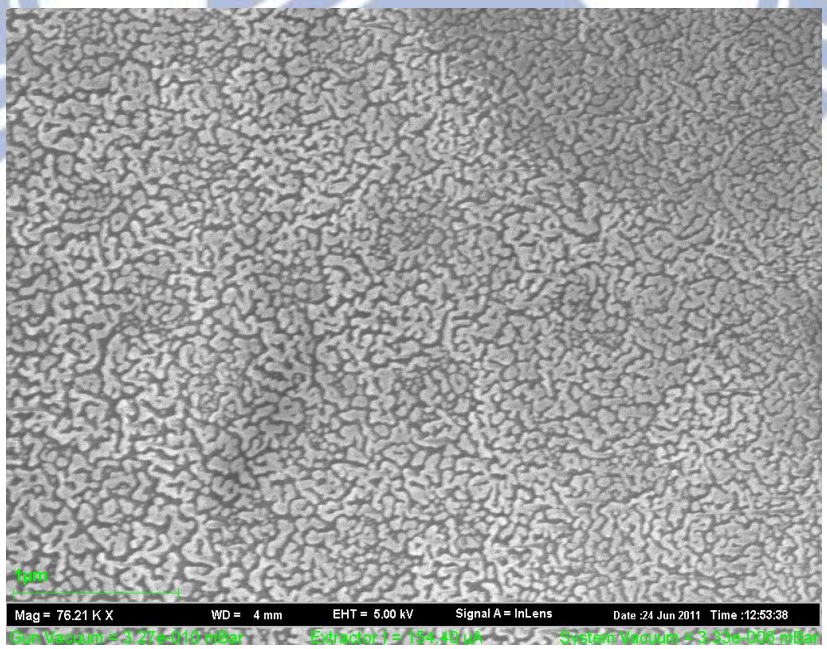

(b)Enlargement of the pattern. Au seems that had been melting and then solidified again by 80 MHz laser.

5-2 The results of Z-scan with an 1kHz laser : Ablation hole

In order to prevent thermal-lens effect, we performed the Z-scan measurement using the Spitfire (Spectra-Physics) laser which is an amplified laser system with the repetition rate 1kHz. The spacing between the laser pulses is 1ms which is much longer than the Au thermal-diffusion time 1μs. Therefore, the thermal-lens effect can be negligible. Figure 5-5 shows that there is no signal even at the input intensity of 4.77 GW/cm^2, which is about 10 times higher than the intensity of MHz laser intensity. It indicates that the thermal-lens effect no longer influence our measurement. However, the morphology study of the excited area shows that there is a permanent damage on sample when the optical intensity above 9.54GW/cm^2 is used.

Figure 5-6 shows the CA Z-scan traces taken at in a sequence of low, high, and again low optical intensity. The first Z-scan trace taken at a low optical intensity shows a flat. The same spot excited at a high intensity shows a peak-valley close-aperture trace, indicating that sample has the characteristic of negative lens. Finally, we reduced the intensity to the initial low value and measured the trace again. However, the trace in Figure 5-6 shows the same peak-valley feature as taken at the high intensity. This result indicates that the excited area is already damaged. Since the pulsewidth and the repetition rate of laser are within the range of non-thermal-effect, the damage in our sample can be explained by an ablation hole.[5-7],[5-8]. Ablation hole can be treated as an approximate shape of a thin diverging lens [see Fig. 5-7]. Once an ablation hole is formed, the sample acts like having a negative n_2 so that self-defocusing of light can be observed even at a low intensity. The results of open-aperture Z-scan traces [Fig. 5-5] show the increase of transmittance at an intensity of 19.05 GW/cm^2, which also supports the presence of the ablation hole. The SEM images in Fig. 5-8 confirm the presence of ablation holes, in which many Au nanoparticle is shell off in the impact region. Obviously, SEM images of 1 kHz and 80 MHz are different. For the 80MHz

laser being a source, the spacing of pulse about 12.2ns is much shorter than thermal-diffusion time $t_c \sim 1\mu s$, so it constantly heats the Au particles. Once the temperature reaches the melting point of Au, the nanostructure is destroyed. For the measurement with the 1 kHz laser, the peak power is so high to cause the ablation of Au nanoparticle. At a lower intensity, no change in transmittance is observed for both CA and OA Z-scan measurements.

The Z-scan measurement has been a very popular technique for measuring third-order nonlinearity of materials. However, in this chapter, we demonstrated that thermal-lens effect or ablation hole can mimic the third-order nonlinear optical effect. Even when the limits of the Z-scan measurement in the pulsewidth and the repetition rate of light source are satisfied, the intensity of laser should be controlled below the ablation limit.

Fig. 5-5 (a) open-aperture Z-scan trace for 1-layer nanoparticles. (b) close-aperture Z-scan trace for 1-layer nanoparticles.

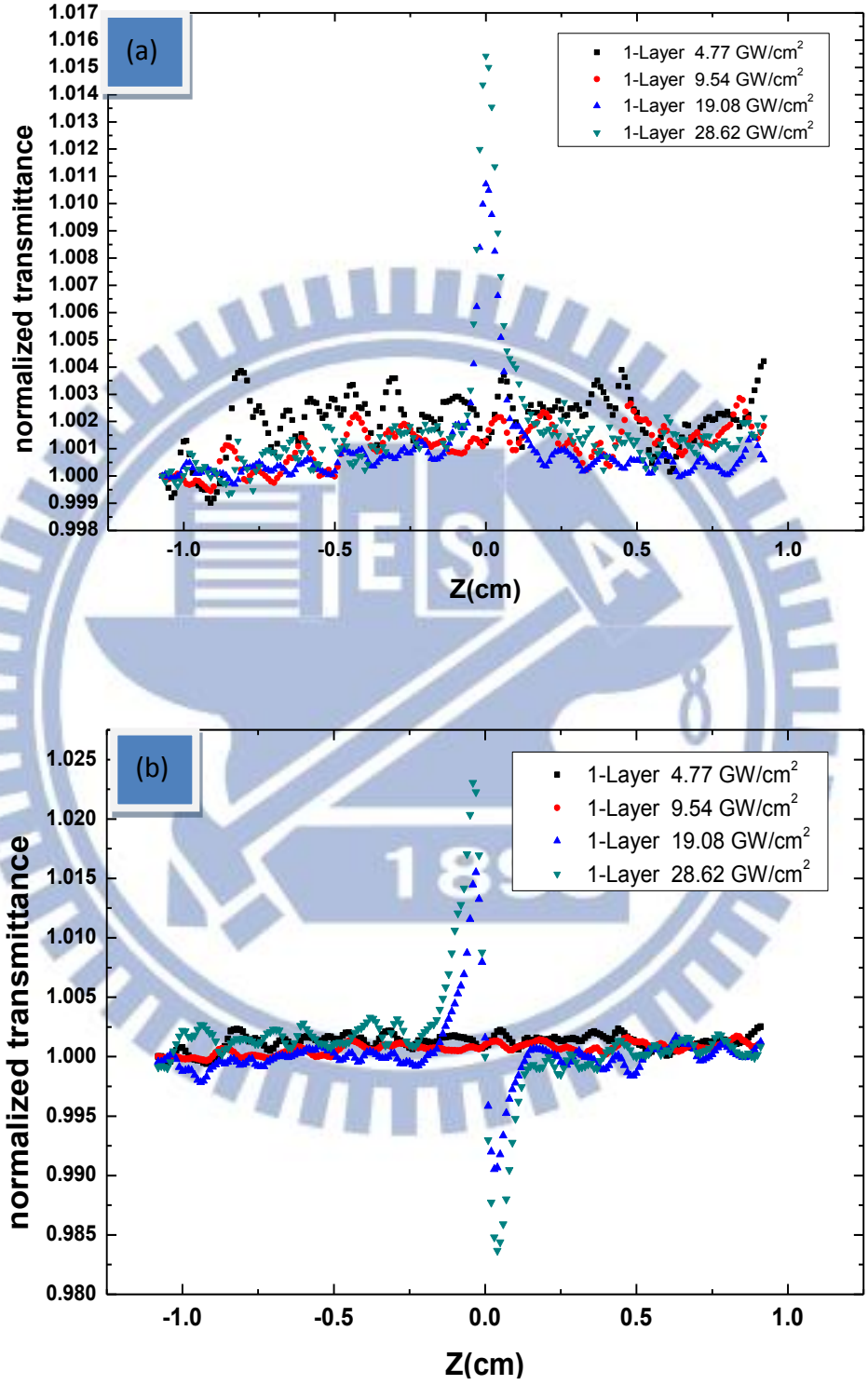

Fig. 5-5 (c) open-aperture Z-scan trace for 2-layer nanoparticles. (d) close-aperture Z-scan trace for 2-layer nanoparticles.

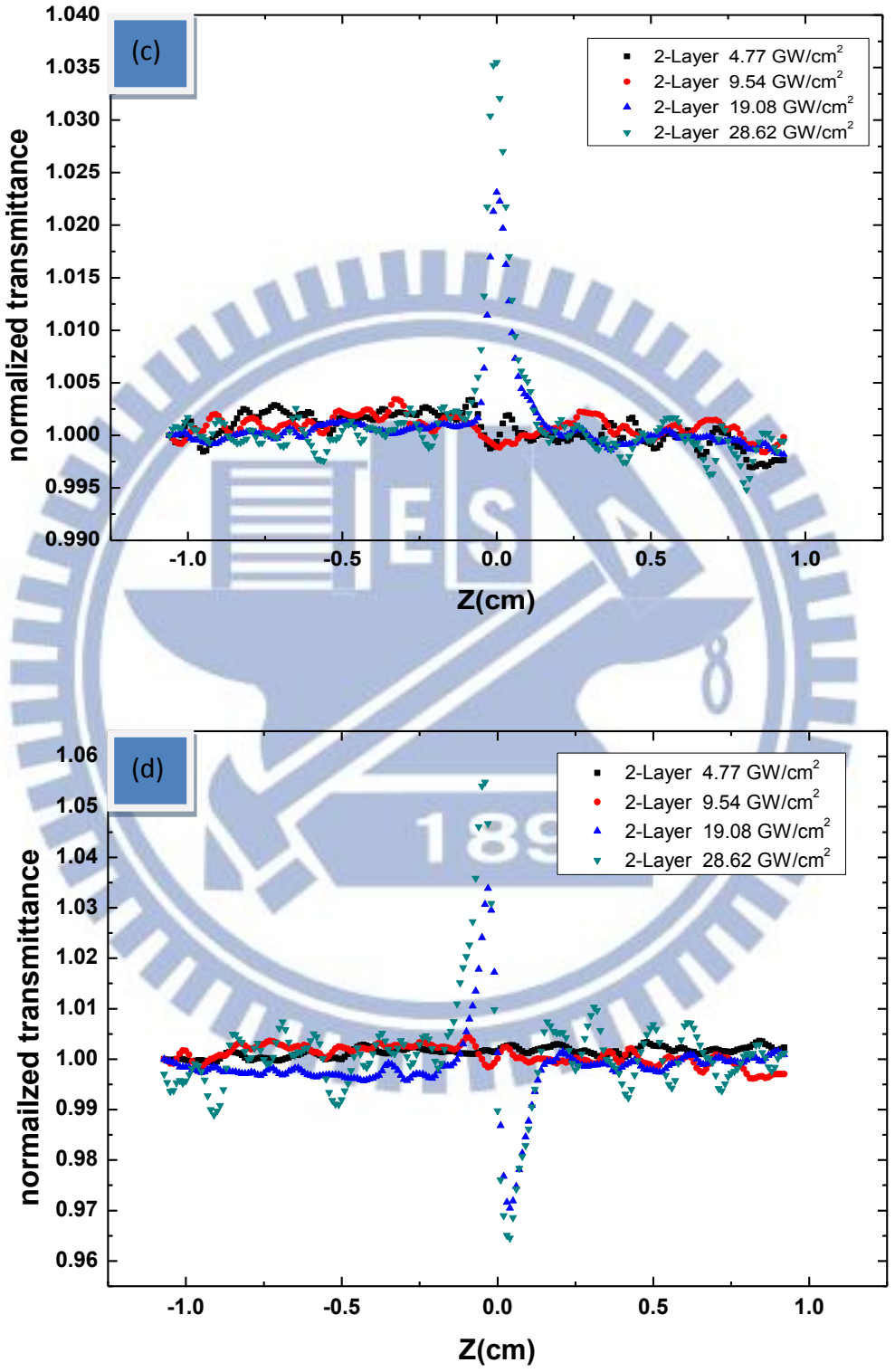

Fig. 5-5 (e) open-aperture Z-scan trace for 3-layer nanoparticles. (f) close-aperture Z-scan trace for 3-layer nanoparticles.

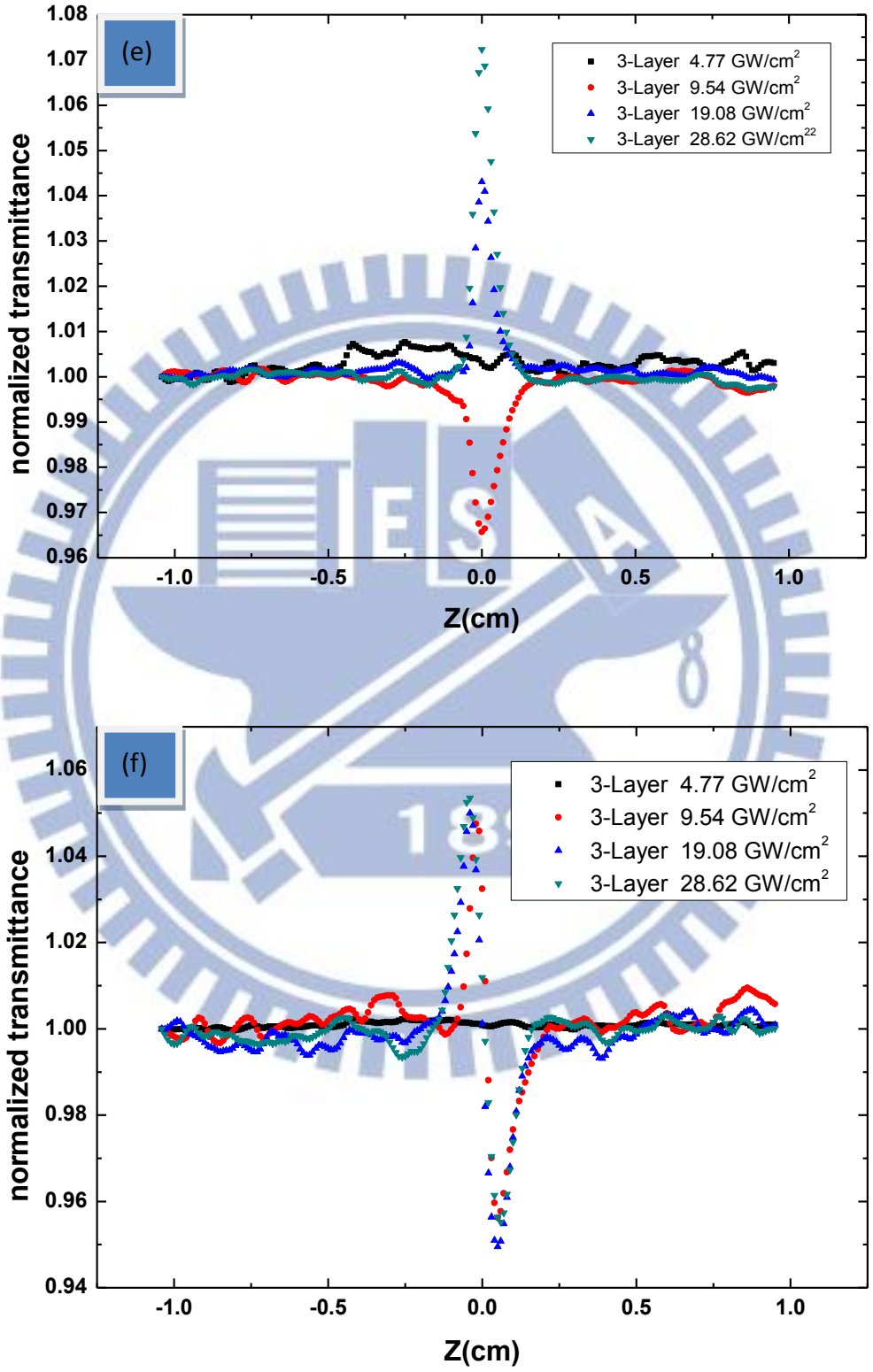

Fig. 5-5 (g) open-aperture Z-scan trace for 5-layer nanoparticles. (h) close-aperture Z-scan trace for 5-layer nanoparticles.

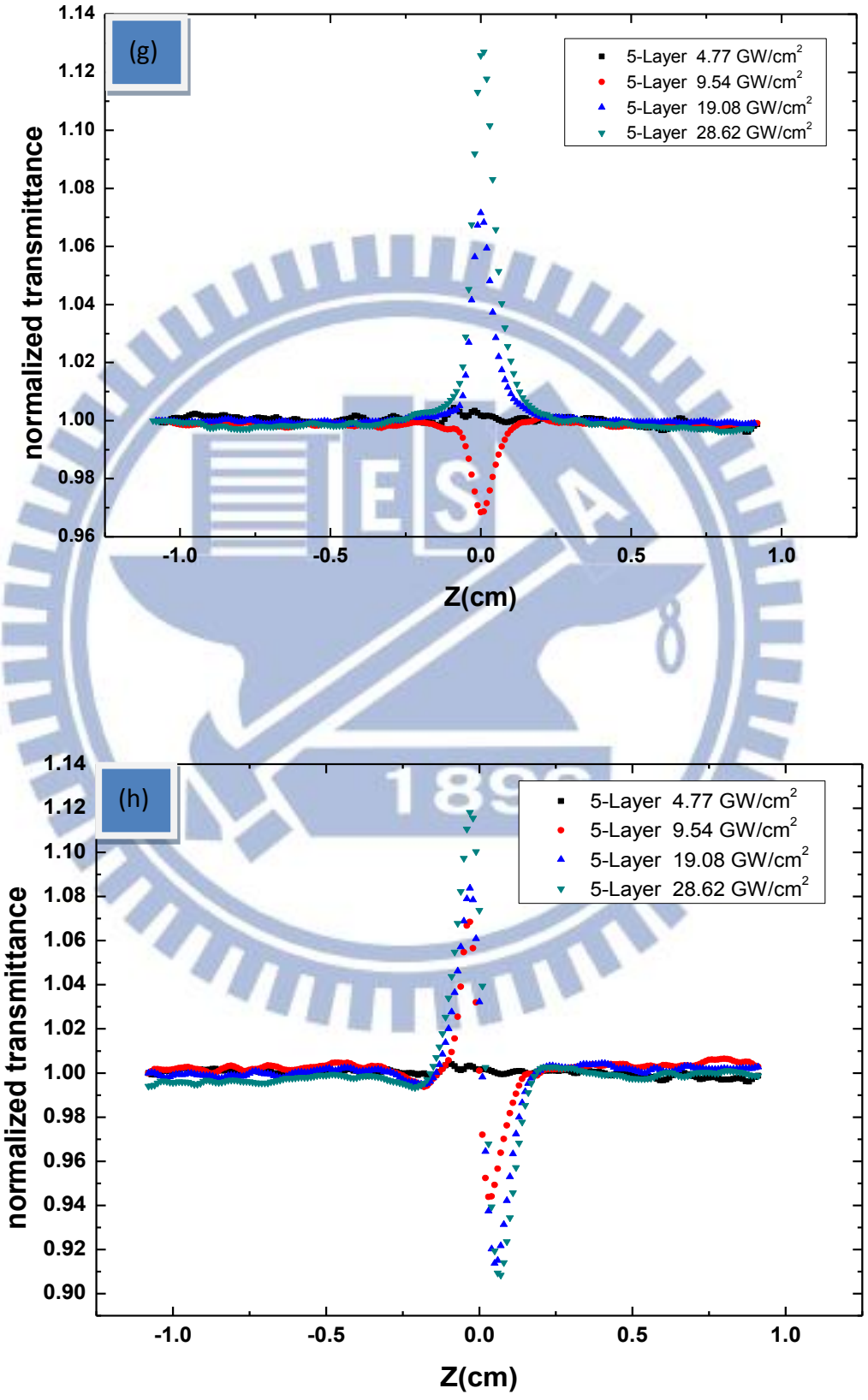

Fig. 5-5 (i) open-aperture Z-scan trace for 10-layer nanoparticles. (j) close-aperture Z-scan trace for 10-layer nanoparticles.

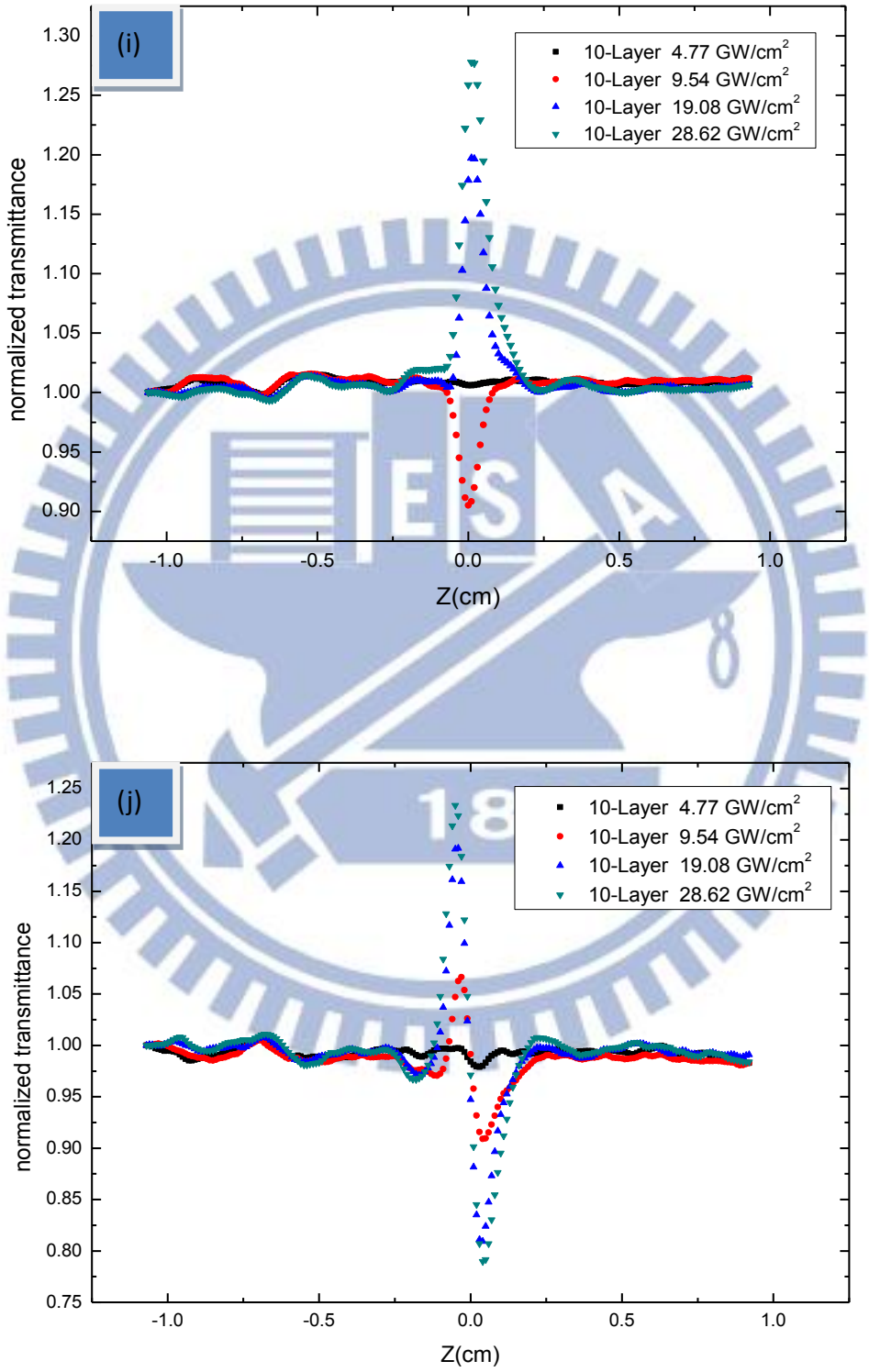

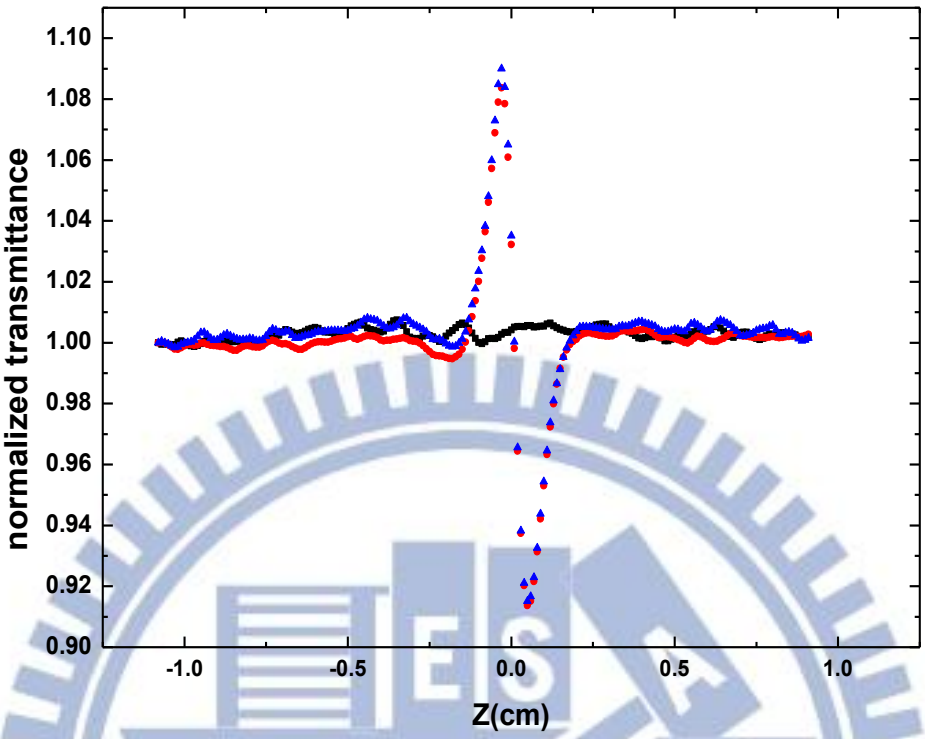

Fig. 5-6 Black line is Z-scan traces at 4.77GW/cm^2(first time) that shows no signal. Red line is Z-scan traces at 19.08GW/cm^2. Blue line is Z-scan traces at 4.77GW/cm^2 afterward excited by 19.08GW/cm^2 which is inconsistent with first measurement indicates a permanent damage is on the sample.

Fig. 5-7 The shadow part is ablation region. It causes spatial dependence of the linear refractive index n_0. When sample is brought closer to the focus, most part of beam begins to diffract and produce intensity variation in far field.

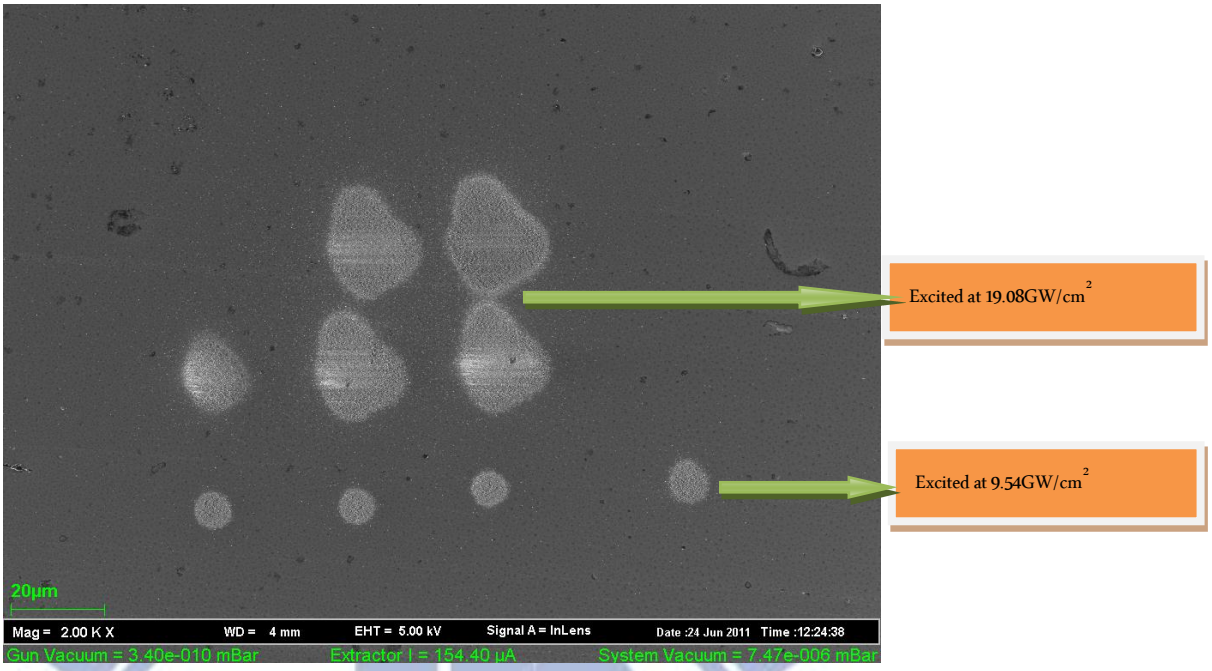

Fig. 5-8 (a)Using the 1kHz laser to make the ablation hole pattern on the 5-layers Au nanoparticle. Four of smaller holes are exited at 9.54GW/cm^2. The others are excited at 19.08GW/cm^2. Both of these are exposed 6 minutes.

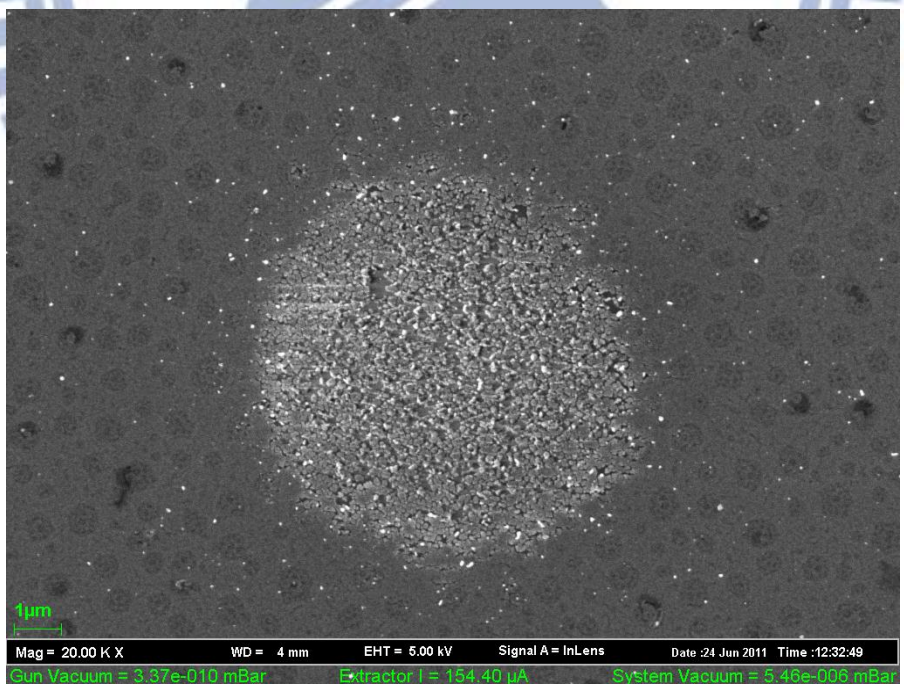

(b)Enlargement of ablation hole exited at 9.54GW/cm^2.

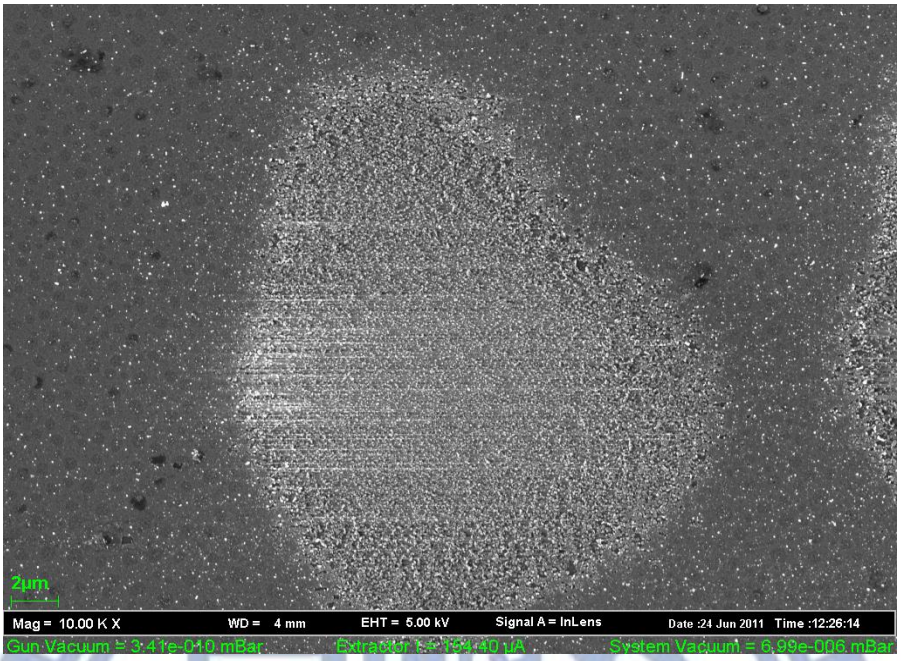

(c)Enlargement of ablation hole exited at 19.08GW/cm^2.

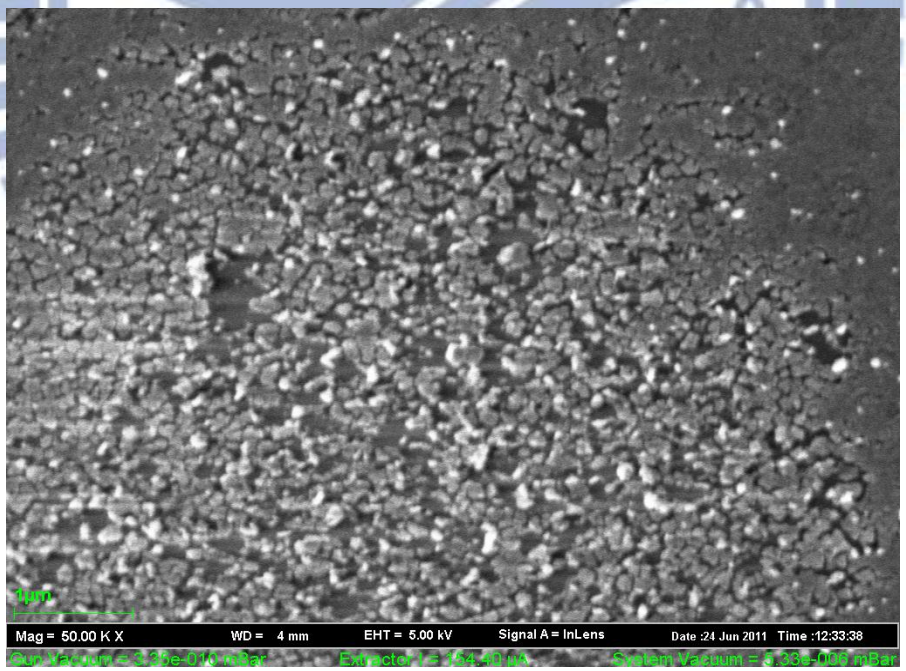

(d)Au nanoparticle shelling off can be clearly observed .

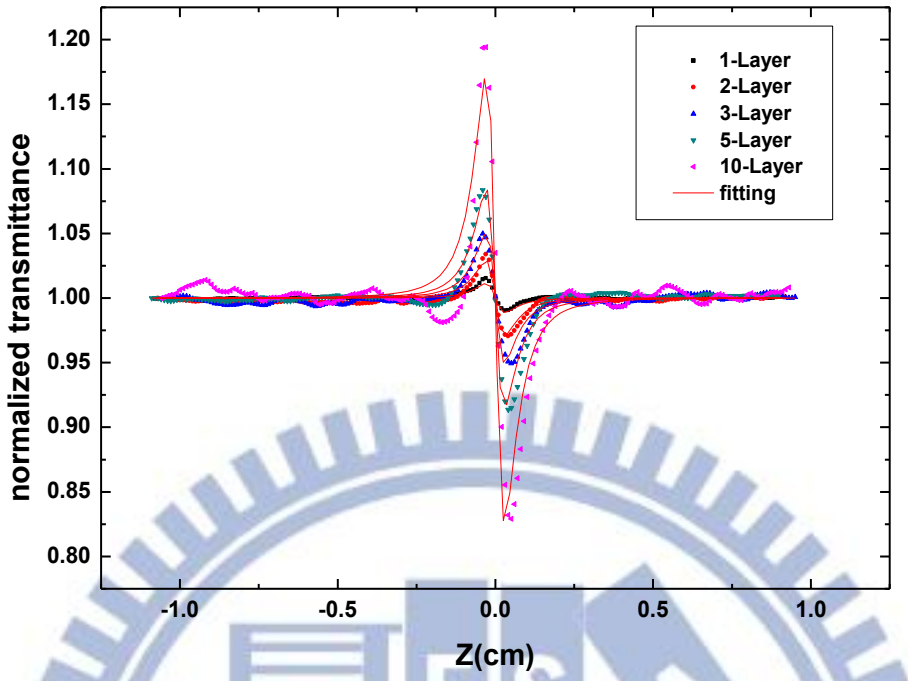

Fig. 5-9 The close-aperture Z-scan traces for different layers of Au nanoparticles fitted by eq. (2-13). Although these signal are not caused by nonlinear response, they can still be well fitted.

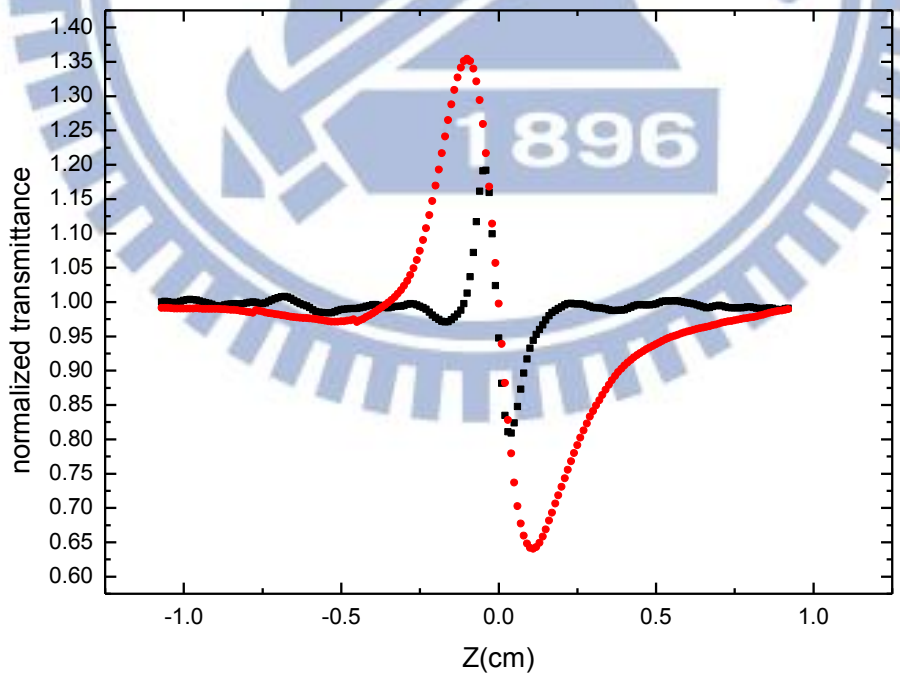

Red line	repetition rate: 80MHz, optical intensity: 0.4GW/cm^2
Black line	repetition rate: 1kHz, optical intensity: 19.08GW/cm^2

Fig. 5-10 Z-scan traces are different between kHz and MHz lasers measurement.

Chapter 6 Conclusions and future plan

Optical nonlinearity of InN thin film was investigated by the Z-scan technique. We obtained the third-order nonlinear refractive index of InN film $n_2=(5.84 \pm 0.2) \times 10^{-11}$, nonlinear absorption coefficient $\beta=-(2.12 \pm 0.06) \times 10^{-6}$ at the wavelength 800 nm and $n_2=(1.86 \pm 0.1) \times 10^{-10}$, $\beta= (1.65 \pm 0.01) \times 10^{-5}$ at the wavelength 1550 nm. InN thin film shows self-focusing at both wavelengths in close-aperture Z-scan. Although the photon energies of both wavelenghts are higher than InN band gap, we observed the absorption saturation behavior at 800nm, while the absorption increases at 1550nm in open-aperture Z-scan scheme. SA at 800 nm is attributed to the band filling effect and the increase in absorption is due to the band-gap renormalization effect, significant at the bottom of the conduction band. In order to clarify our observation, the Z-scan measurement at different wavelengths, near the bandgap energy, may be necessary.

In the Z-scan measurement of Au nanoparticles at 800nm, although we could not obtain the nonlinear coefficient, we found that the thermal-lens effect and ablation hole can mimic the optical nonlinear response of the Z-scan signal. In order to avoid the ablation of Au nanoparticles, we performed the Z-scan measurement at a low intensity, but the signal was undetectably small. Despite the L-mode resonance becomes obvious as the layer number increases, the nonlinear effect may be still too small to be detected at 800 nm. Therefore, we will perform the Z-scan measurement at the resonance wavelength of bulk Au 530 nm. We expect to observe the transition of the nonlinear coefficients from 2D values to bulk values as the number of layers increases. Although there may be a difficulty in fabrication, growing Au nanoparticle superlattice on other substrate materials which have higher thermal conductivities can be beneficial in reducing the thermal-related effect..

Reference

[1-1] J. E. Midwinter, editor. Photonics in Switching. Quantum Electronics - Principles and Applications. Academic Press, (1993).

[1-2] G. S. He, L.-S. Tan, Q. Zheng, and P. N. Prasad. Multiphoton absorbing materials: Molecular designs, characterizations, and applications. Chemical Review, **108**,1245–1330, (2008).

[1-3] M. Sheik-Bahae, A. A. Said, T.-H. Wei, D. J. Hagan, and E. W. Van Stryland, IEEE J. Quantum Electron. **26**, 760, (1990).

[1-4] M.-H. Lin, H.-Y. Chen, and S. Gwo, "Layer-by-Layer assembly of three-dimensional colloidal supercrystals with tunable plasmonic properties," J. AM CHEM. SOC. **132**, 11259, (2010).

[1-5] Bahaa E. A. Saleh, Malvin Carl Teich, "Fundamentals of Photonics," (2010)

[1-6] Robert W. Boyd," Nonlinear Optics", (1992)

[1-7] Claude Rulli`ere, "Femtosecond Laser Pulses Principles and Experiments Second Edition," (2003)

[2-1] A.A. Said, M. Sheik-Bahae, D.J. Hagan, T.H. We, J. Wang, J. Young, E.W. Van Stryland, J. Opt. Soc. Am. B 9, 405, (1992)

[2-2] K.S. Bindra , S.M. Oak, K.C. Rustagi "Intensity dependence of Z-scan in semiconductor-doped glasses for separation of third and fifth order contributions in the below band gap region," Optics Communications **168,** 219–225, (1999)

[3-1] 王蒼祺, “Determination of optical nonlinearity of ZnTe by Z-scan technique,” NCTU thesis, June 2001

[4-1] E Fazio1, A Passaseo2, M Alonzo1, A Belardini1, C Sibilia1, M C Larciprete1 and M Bertolotti1 “Measurement of pure Kerr nonlinearity in GaN thin films at 800 nm by means of eclipsing Z-scan experiments,” J. Opt. A: Pure Appl. Opt. **9,** L3–L4, (2007)

[4-2] Sheik-Bahae, M. Said, A. A., and Van Stryland, E. W., *Opt. Lett.* 14, 955, (1989)

[4-3] S. KRUKOWSKI, A. WITEK , J. ADAMCZYK , J. JUN , M. BOCKOWSKI , I. GRZEGORY , B. LUCZNIK , G. NOWAK , M. WROBLEWSKI , A. PRESZ , S. GIERLOTKA , S. STELMACH , B. PALOSZ , S. POROWSKI and P. ZINN “Thermal properties of Indium Nitride,” 1. Phys. Chem Solids Vol **59**. No. 3. pp. X39-295. 1998

[4-4] H. Ahn, C.-H. Shen, C.-L. Wu, and S. Gwo, “Spectroscopic ellipsometry study of wurtzite InN epitaxial films on Si.111. with varied carrier concentrations,” Appl. Phys. Lett. **86**, 201905, (2005)

[4-5] Francesco G. Della Corte, Giuseppe Cocorullo, Mario Iodice, and Ivo Rendina “Temperature dependence of the thermo-optic coefficient of InP, GaAs, and SiC from room temperature to 600 K at the wavelength of 1.5 mm,” Appl. Phys. Lett., Vol. **77**, No. 11, (2000)

[4-6] David R. Cassidy and Graham H. Cross “Universal method to determine the thermo-optic coefficient of optical waveguide layer materials using a dual slab waveguide,” Appl. Phys. Lett. **91**, 141914 (2007)

[4-7] Tsong-Ru Tsai, Tsung-Han Wu, Jung-Cheng Liao, Tai-Huei Wei, Hai-Pang Chiang,Jih-Shang Hwang, Din-Ping Tsai, and Yang-Fang Chen “Characterization of nonlinear absorption of InN epitaxial films ith femtosecond pulsed transmission *Z*-scan measurements,” J. Appl. Phys. **105**, 066101, (2009)

[4-8] A. B. Miller, C. T. Seaton, M. E. Prise, and S. D. Smith, Phys. Rev. Lett. **47**, 197, (1981)

[5-1] Mauro Falconieri, “Thermo-optical effects in Z-scan measurements using high-repetition-rate lasers,” J. Opt. A: Pure Appl. Opt. **1,** 662–667, (1999)

[5-2] R. de Nalda, R. del Coso, J. Requejo-Isidro, J. Olivares, A. Suarez-Garcia, J. Solis, and C. N. Afonso, ” Limits to the determination of the nonlinear refractive index by the Z-scan method,” J. Opt. Soc. Am. B Vol. **19**, No. 2, (2002)

[5-3] T. Tokizaki, A. Nakamura, S. Kaneko, K. Uchida, S. Omi, H.Tanji, and Y. Asahara, ‘‘Subpicosecond time response of third order optical nonlinearity of small copper particles in glass,’’ Appl. Phys. Lett. **65**, 941–943, (1994).

[5-4] M. Falconieri, G. Salvetti, “Simultaneousmeasurement of pure-optical and thermo-optical nonlinearities induced by high-repetition-rate, femtosecond laser pulses: application to CS2,” Appl. Phys. B **69**, 133–136, (1999)

[5-5] J.P. Gordon, R.C.C. Leite, R.S. Moore, S.P.S. Porto, J.R. Whinnery: J. Appl. Phys. **36**, 3, (1965)

[5-6] K. Fedus, G. Boudebs, C. B. de Araujo, M. Cathelinaud, F.Charpentier, and V. Nazabal, “Photo-induced effects in thin films of Te20As30Se50 glass with nonlinear characterization,” Appl. Phys. Lett. **94**, 061122, (2009).

[5-7] B. M. Patterson, W. R. White, T. A. Robbins, and R. J. Knize, “Linear optical effects in Z-scan measurements of thin films,” Appl. Opt. **37**, 1854–1857, (1998).

[5-8] Georges Boudebs* and Kamil Fedus, “Linear optical characterization of transparent thin films by the Z-scan technique,” APPLIED OPTICS / Vol. **48**, No. 21 / 20 July 2009